1976

A magnetometer data acquisition system.

Xefteris, Constantine Louis

Monterey, California. Naval Postgraduate School

A MAGNETOMETER DATA ACQUISITION SYSTEM

Constantine Louis Xefteris

NAVAL POSTGRADUATE SCHOOL
Monterey, California

THESIS

A MAGNETOMETER DATA ACQUISITION SYSTEM

by

Constantine Louis Xefteris

June 1976

Thesis Advisor: G. L. Sackman

SECURITY CLASSIFICATION OF THIS PAGE (When Data Entered)

REPORT DOCUMENTATION PAGE		READ INSTRUCTIONS BEFORE COMPLETING FORM
1. REPORT NUMBER	2. GOVT ACCESSION NO.	3. RECIPIENT'S CATALOG NUMBER
4. TITLE (and Subtitle) A Magnetometer Data Acquisition System		5. TYPE OF REPORT & PERIOD COVERED Master's Thesis June 1976 6. PERFORMING ORG. REPORT NUMBER
7. AUTHOR(s) Constantine Louis Xefteris		8. CONTRACT OR GRANT NUMBER(s)
9. PERFORMING ORGANIZATION NAME AND ADDRESS Naval Postgraduate School Monterey, California 93940		10. PROGRAM ELEMENT, PROJECT, TASK AREA & WORK UNIT NUMBERS
11. CONTROLLING OFFICE NAME AND ADDRESS Naval Postgraduate School Monterey, California 93940		12. REPORT DATE June 1976 13. NUMBER OF PAGES 92
14. MONITORING AGENCY NAME & ADDRESS(if different from Controlling Office) Naval Postgraduate School Monterey, California 93940		15. SECURITY CLASS. (of this report) Unclassified 15a. DECLASSIFICATION/DOWNGRADING SCHEDULE

16. DISTRIBUTION STATEMENT (of this Report)

Approved for public release; distribution unlimited.

17. DISTRIBUTION STATEMENT (of the abstract entered in Block 20, if different from Report)

18. SUPPLEMENTARY NOTES

19. KEY WORDS (Continue on reverse side if necessary and identify by block number)

20. ABSTRACT (Continue on reverse side if necessary and identify by block number)

A system for the analysis of geomagnetic and gradient noise is described. The nominal 176 kHz Larmor frequency output of an optically pumped cesium magnetometer is mixed to a frequency in the 1.2 kHz range and FM tape recorded. The recorded output is applied to a periodmeter, the digital output of which is input to the XDS-9300 computer for analysis and display. The

DD FORM 1 JAN 73 1473 EDITION OF 1 NOV 65 IS OBSOLETE
S/N 0102-014-6601 |
(Page 1)

SECURITY CLASSIFICATION OF THIS PAGE (When Data Entered)

20. Abstract (cont'd)

absolute accuracy of the period measurement is .75 μsec with a resolution of .25 μsec. The RMS noise of the tape recorder was determined to be .667 sec or in the operating frequency range less than 1 Hz or .28 gamma. Externally introduced field disturbances as small as .5 gamma were recorded and displayed, and the response time of the magnetometer determined to be less than 2.5 msec.

A Magnetometer Data Acquisition System

by

Constantine Louis Xefteris
Lieutenant, United States Navy
B.S.E.E., Marquette University, 1971

Submitted in partial fulfillment of the
requirements for the degree of

MASTER OF SCIENCE IN ELECTRICAL ENGINEERING

from the

NAVAL POSTGRADUATE SCHOOL
June 1976

ABSTRACT

A system for the analysis of geomagnetic and gradient noise is described. The nominal 176 kHz Larmor frequency output of an optically pumped cesium magnetometer is mixed to a frequency in the 1.2 kHz range and FM tape recorded. The recorded output is applied to a periodmeter, the digital output of which is input to the XDS-9300 computer for analysis and display. The absolute accuracy of the period measurement is .75 μsec with a resolution of .25 μsec. The RMS noise of the tape recorder was determined to be .667 μsec or in the operating frequency range less than 1 Hz or .28 gamma. Externally introduced field disturbances as small as .5 gamma were recorded and displayed, and the response time of the magnetometer determined to be less than 2.5 msec.

TABLE OF CONTENTS

LIST OF FIGURES

LIST OF TABLES

I. INTRODUCTION

With a continuing interest in magnetic anomaly detection the Naval Postgraduate School has studied geomagnetic noise, first with the proton precession magnetometer and later with the optically pumped rubidium type. In 1972 the school obtained an optically pumped cesium magnetometer with accessories to convert it to a gradiometer. In order to take full advantage of the inherent high frequency response of this magnetometer a data collection system was developed to observe geomagnetic and gradient noise. Figure 1.1 is a block diagram of the system.

A brief introduction to the earth's magnetic field and other measuring instruments is presented first followed by a description of the system developed.

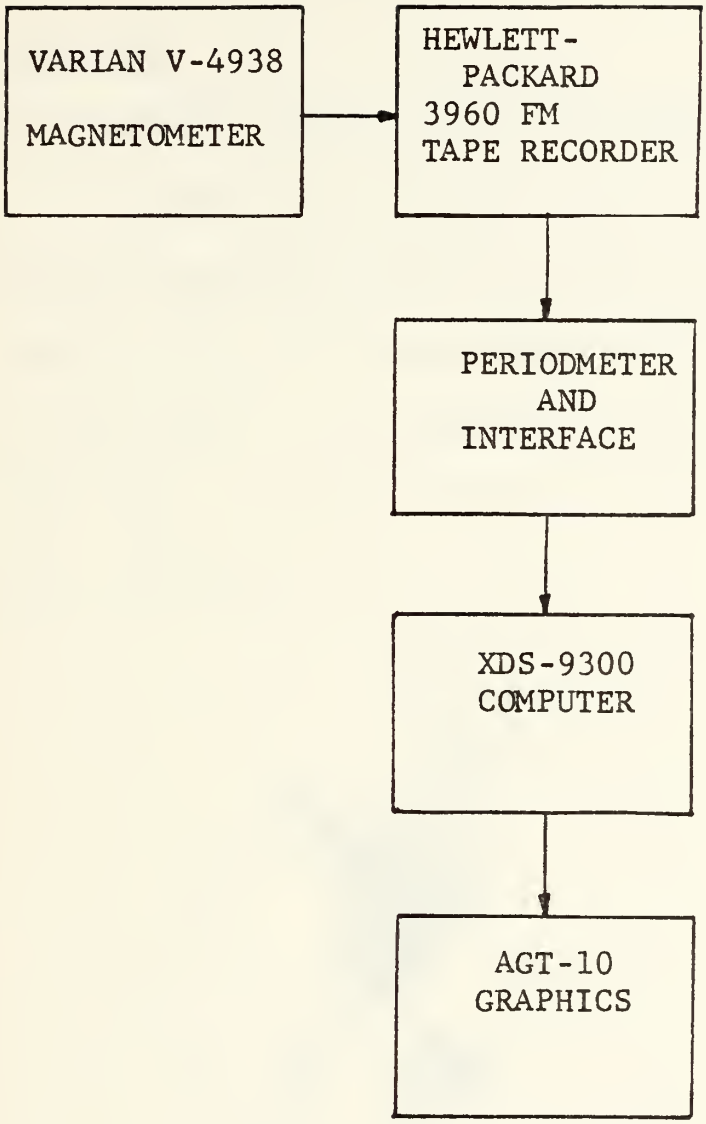

Figure 1.1 System Block Diagram

II. THE MEASUREMENT FIELD

A. MAIN FIELD

World magnetic surveys both at ground level and more recently by satellite indicate that the principal source of the main geomagnetic field is beneath the earth's crust. Approximately 90% of the main field exhibits characteristics roughly equivalent to the field of a terrestrially centered short bar magnet or dipole inclined at 11.5° to the axis of rotation. See Figure 2.1.

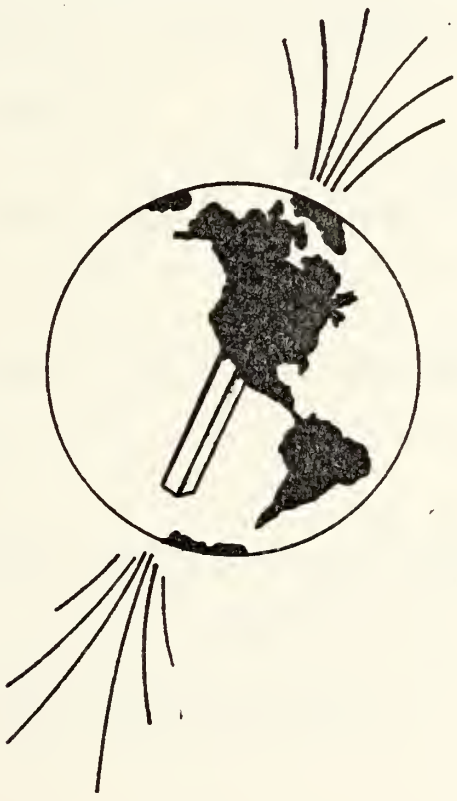

Figure 2.1 Dipole Appearance of Geomagnetic Field

The field strength is approximately 60 kilogammas in the polar regions, 30 kilogammas in the equatorial region, and 50 kilogammas in the neighborhood of 37^{o} North latitude on the west coast of the United States. Figure 2.2 shows a world chart of the total intensity of the surface field.[1] The main field has a slow secular change of about .1% per year and it is a regional phenomenon which may reach .3% in certain regions.

B. UNITS

The customary unit of measurement is the gamma, regarded interchangeably as a unit of induction (gauss) or of magnetic intensity (oersted).

1 gamma is 10^{-5} gauss (10^{-9} tesla)

or

1 gamma is 10^{-5} oersted ($10^{-2}/4\pi$ ampere turn/meter)

C. ELEMENTS

The various elements of the magnetic field are shown in Figure 2.3. They are defined as:

X North South Component

---

[1]Air Force Cambridge Research Laboratories, Handbook of Geophysics and Space Environments, p. 11-11, 1965.

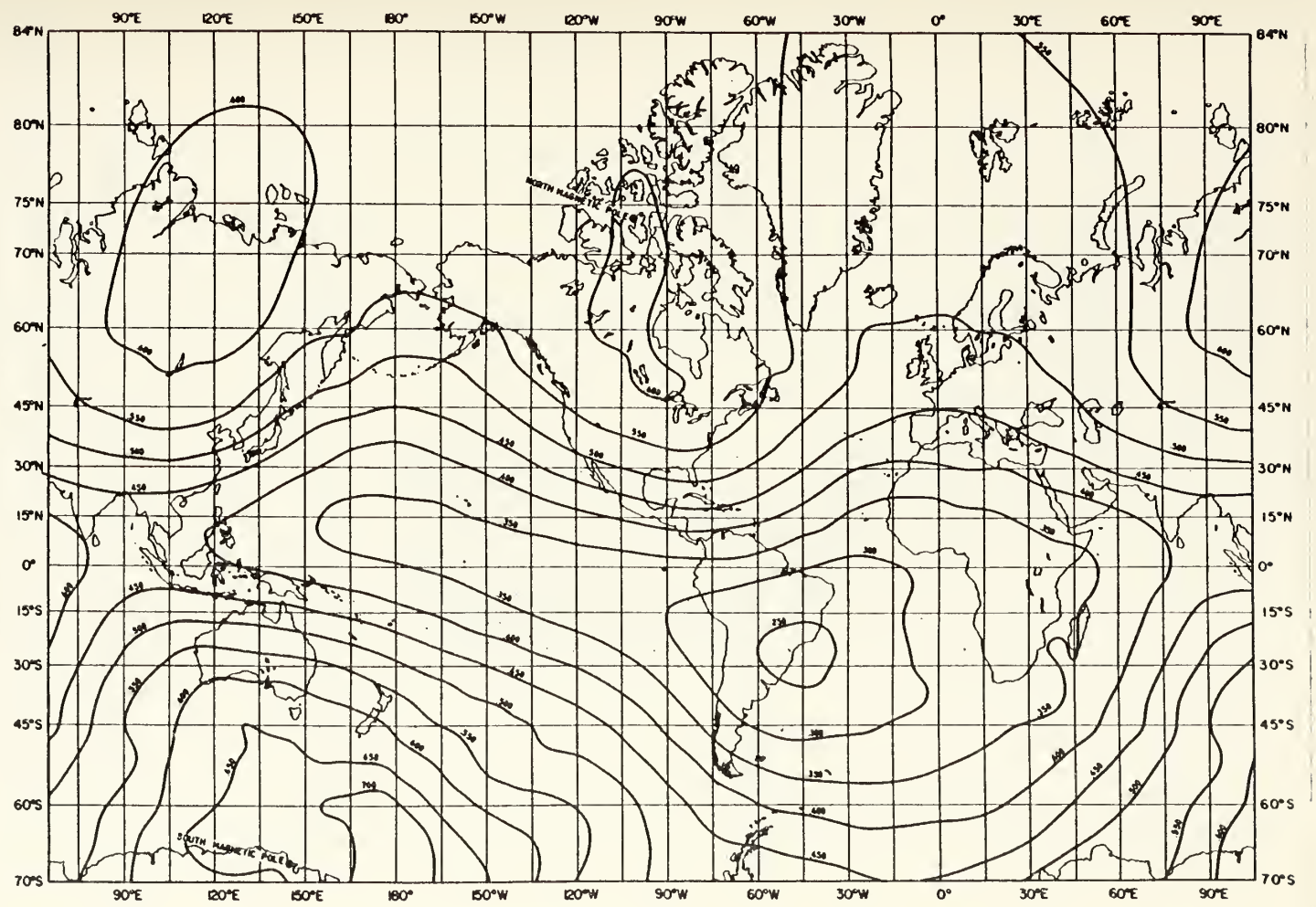

Figure 2.2 World Magnetic Chart

Y East West Component

Z Vertical Intensity

D Declination

H Intensity of the Horizontal Component

F Total Intensity

I Inclination or Dip

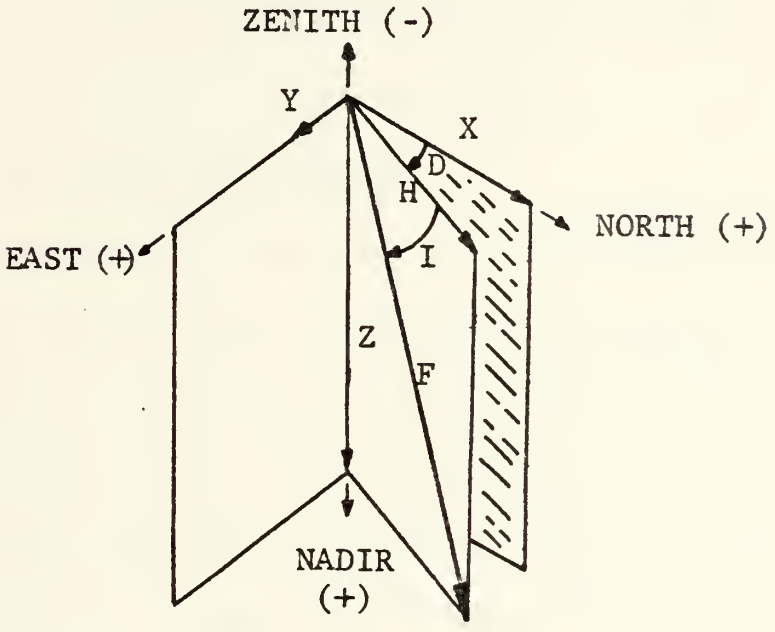

Figure 2.3 Elements of the Field

In terms of the more familiar bar magnet: A magnet perfectly free to turn in any direction would show the vector direction of the field. It is almost impossible to suspend a magnet like that so two are used. One with

a vertical axis (compass) and one with a horizontal axis (dip needle). The compass shows the direction of the horizontal component H, and when properly oriented the dip needle shows the inclination or dip.

D. TIME VARIATIONS

The time variations of the geomagnetic field can be broadly categorized into quiet variation fields, disturbed variation fields, and micropulsations.

1. Quiet Variation Fields

Geomagnetic records occasionally show a very smooth trace that clearly indicates a pattern of daily variation with respect to solar local time. This pattern is named "solar quiet day variation" and denoted Sq. There is also a lunar daily variation, denoted L, but it is much weaker and more variable. Both the Sq and L variations result from the dynamo action of the atmosphere, a complex phenomenon of convective motions caused by the solar heating of the upper atmosphere under the influence of the earth's magnetic field. These convective motions induce ionospheric currents and electric currents in the earth itself, both of which cause magnetic variations. The effects of electric current induction within the earth are sometimes referred

to as geological disturbances because the amount of induction is dependent on the composition of the earth's crust. For example, the intensity of induced currents in the ocean is higher than those in the continental crustal layers.

Figure 2.4 shows the Sq variation recorded in Monterey during a quiet period.

2. Disturbed Variation Fields

Any fluctuation other than the quiet day solar and lunar variations can be called a magnetic disturbance. Other than disturbances directly attributable to a solar flare or fluctuations produced by upper atmospheric irregular motions, all are caused originally by disturbed solar plasma and may therefore be generally classified as one family. The term magnetic storm is reserved to apply to a relatively severe, long lasting disturbance with recognizable features, but all other irregular variations deviating from the Sq and L variations are termed simply magnetic disturbances. They have durations lasting from 100 hours to several minutes. Figure 2.5 shows a magnetic disturbance recorded in Monterey that immediately followed the Sq variations shown in Figure 2.4.

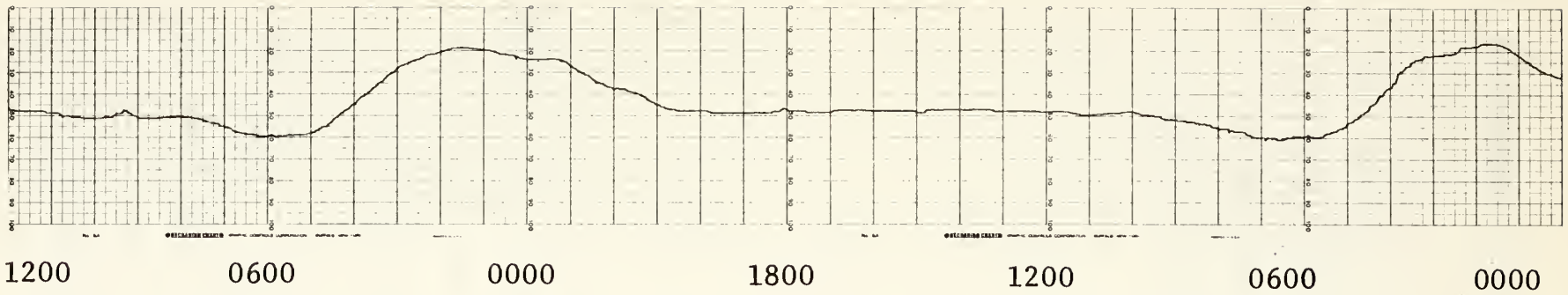

Figure 2.4 Sq Variations, 100 Gammas Full Scale

Figure 2.5 Magnetic Disturbances, 100 Gammas Full Scale

3. Geomagnetic Micropulsations

Geomagnetic micropulsations are field variations with periods ranging from .2 seconds to approximately 10 minutes. A terminology recommended by the International Association of Geomagnetism and Aeronomy is pc for pulsation continuous and pi for pulsation irregular. The period range for these are:

pc 1	.2-5 sec
pc 2	5-10 sec
pc 3	10-45 sec
pc 4	45-150 sec
pc 5	150-600 sec
pi 1	1-40 sec
pi 2	40-150 sec

A general picture of the geomagnetic field in the lower frequencies is shown in Figure 2.6.

Pc 1 pulsations have very small amplitude, between .01 and .1 gamma and have a sinusoidal and beating form. The pulsations appear in bursts and usually last approximately 30 minutes. They have been identified by their appearance and because there is a direct relationship between their reoccurrence period and mid-frequency. No seasonal or latitude dependence has been identified but

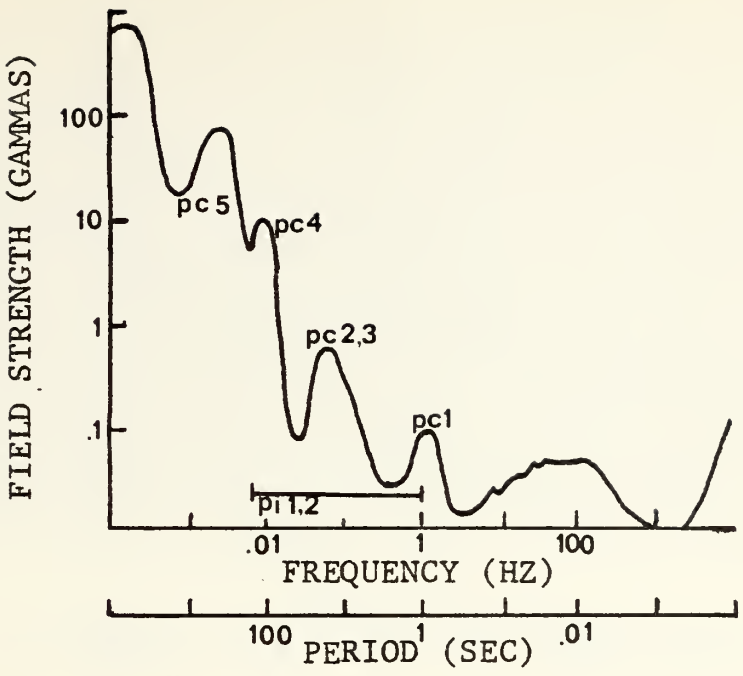

Figure 2.6 Geomagnetic Micropulsation Spectrum

there is a diurnal variation in the mid-frequency events, high frequency events occur in post midnight hours, and low frequency events in the early afternoon. Figure 2.7 is a record of a pc 1 micropulsation observed in Monterey.

Figure 2.8 shows the typical form of the pc 2,3 pulsations. They also exhibit a sinusoidal and beating character similar to the pc 1 type but their amplitude is slightly greater, usually .5 gamma. The duration of the signals seems to be related only to the sensitivity of the detector, which has lead to the hypothesis that when no signal is observed the pulsation is not completely absent

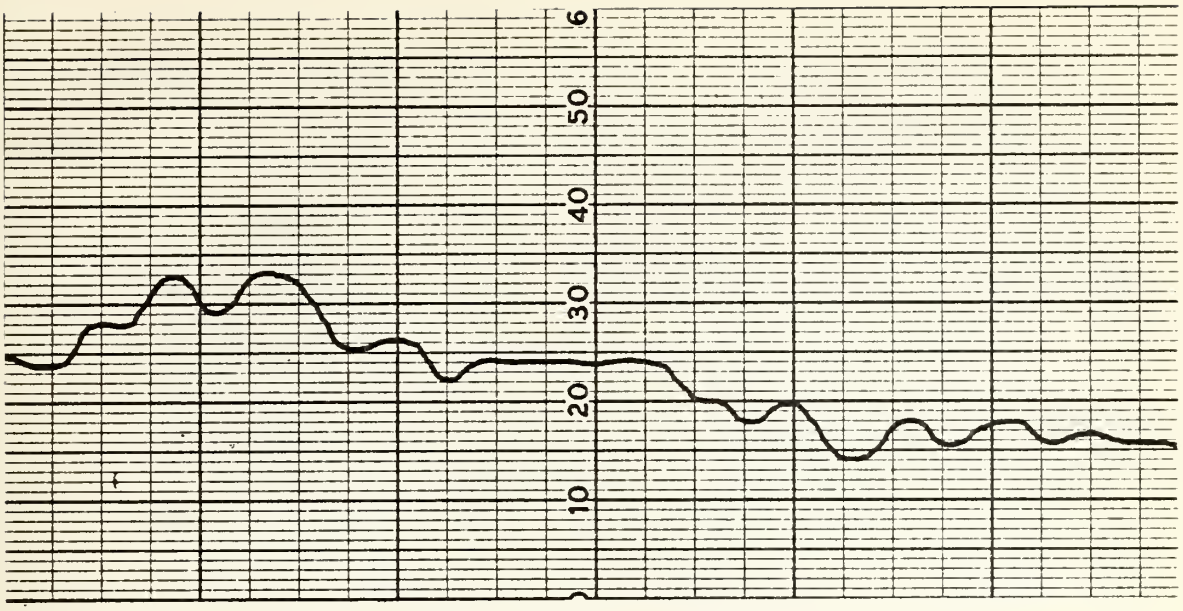

Figure 2.7 Pc1 Micropulsation;
1.8 gammas full scale; 45 second record

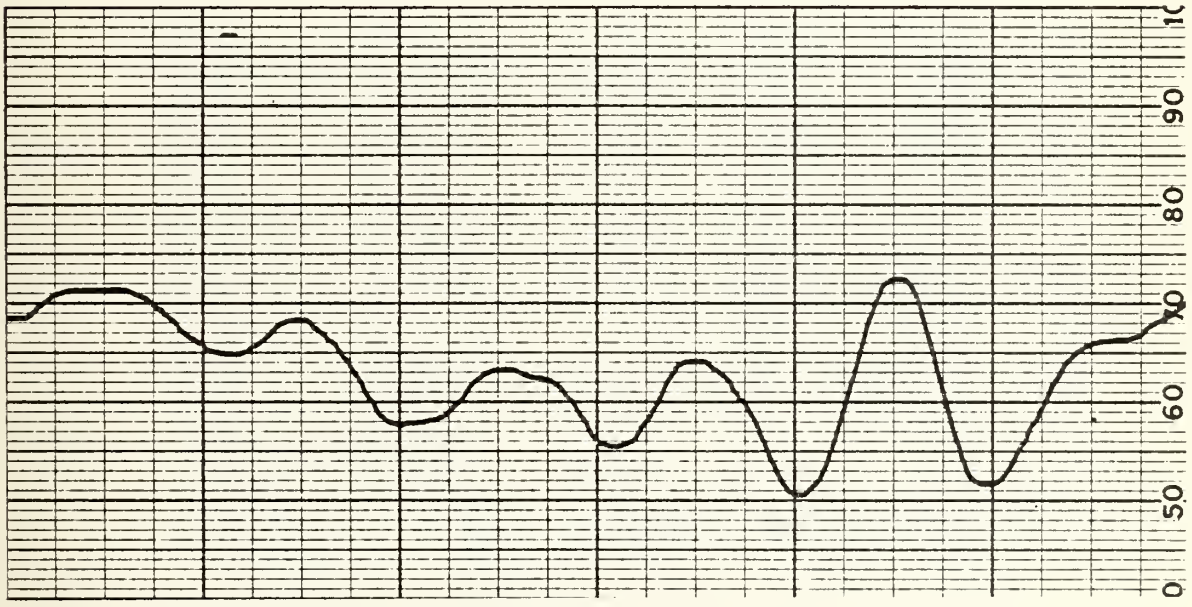

Figure 2.8 Pc 2,3 Micropulsation;
1.8 gammas full scale; 45 second record

but rather too weak to be detected. Pc 2,3 events occur mainly during daylight hours and have a maximum near noon. The average period undergoes a diurnal variation, being a maximum at midday. They also have a 27 day (solar rotation) periodicity and a slight seasonal variation.

As seen in the typical pc 4 record shown in Figure 2.9, these micropulsations slowly rise to a maximum of between 5 and 20 gammas and then symmetrically decay. The average signal lasts about one hour. In mid-latitudes a daytime occurrence pattern can be observed but the period is shorter in the daytime than at night, the opposite of the pc 2,3.

The longest period variations, pc 5, display amplitudes from 10 to hundreds of gammas. Their form is again sinusoidal and they may last from several minutes to several hours. The largest amplitudes are observed in the auroral zone and the occurrences have a direct relationship with auroral zone phenomena.

The class of micropulsations in the 2 to .005 Hz range with irregular form and a close relationship to upper atmospheric and auroral zone phenomena have been designated pi 1,2. Their amplitudes vary greatly, the larger sometimes being called micropulsation storms. Figure 2.10 shows the irregular appearance.

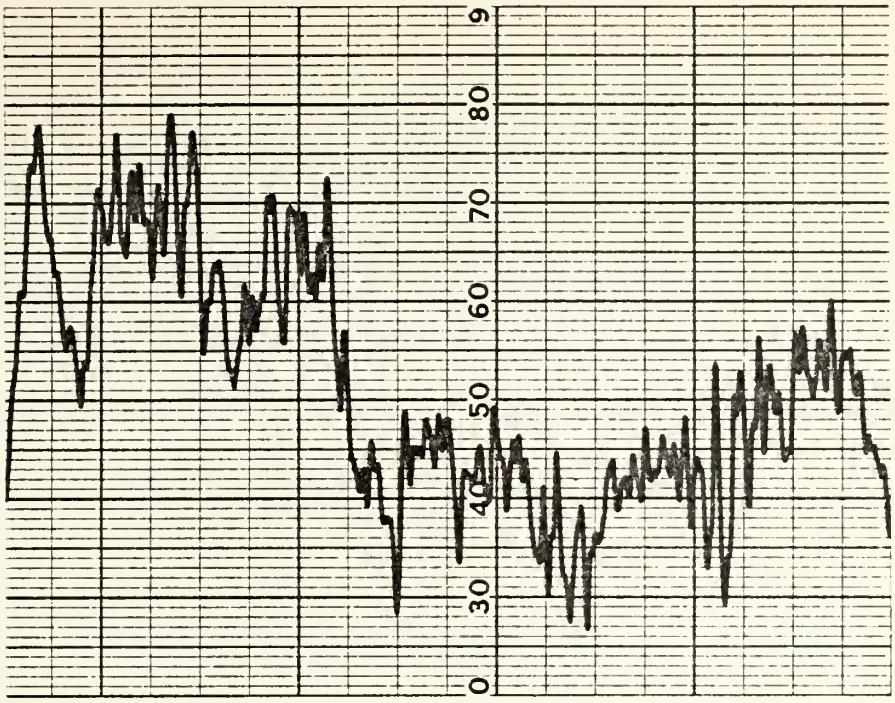

Figure 2.9 Pc4 Micropulsation;
7 gammas full scale; 6 minute record

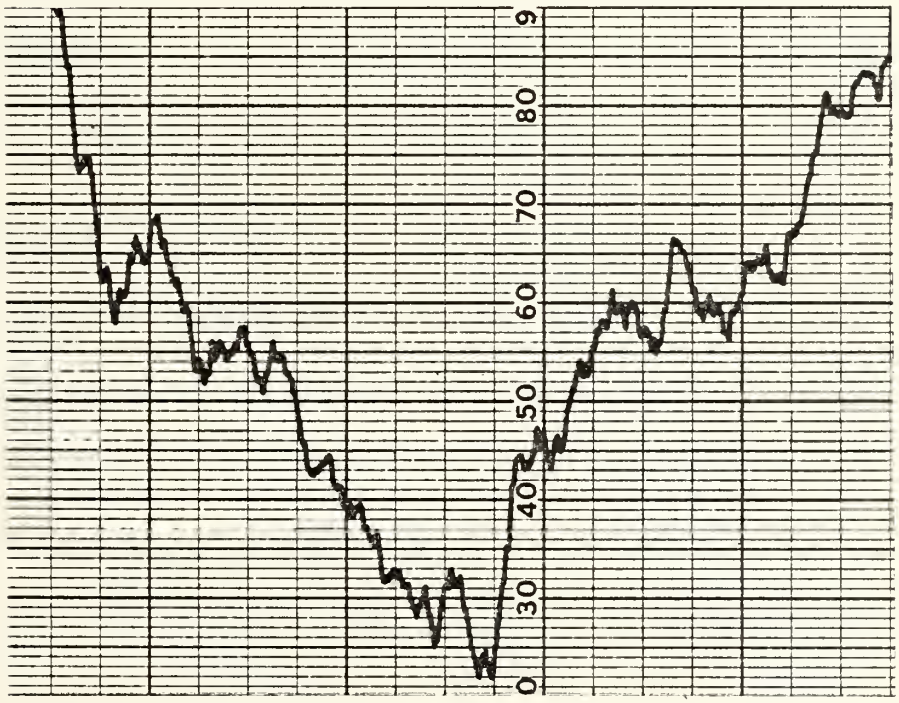

Figure 2.10 Pi2 Micropulsation;
7 gammas full scale; 6 minute record

III. MEASURING INSTRUMENTS

Today a wide range of devices are available for measuring the magnetic field, ranging from the extremely old magnetized needle to the newer superconducting quantum types. The major considerations in the selection of a device in a non-observatory application are sensitivity, accuracy, frequency response, mobility, and reliability. Three types of magnetometers that have developed with these considerations as guidelines are the fluxgate, optically pumped resonance, and superconducting quantum. They will be described and a comparison of the different varieties and other types is given in Table I.

A. FLUXGATE

A fluxgate magnetometer, sometimes referred to as a saturable core or saturable inductor, measures magnetic fields by utilizing the variation of permeability with intensity of magnetization in a ferromagnetic core. An easily saturable ferromagnetic core of high permeability is driven cyclically into saturation by an applied magnetic field. In the absence of an external field, which is usually dc or very low ac and small with respect to the

applied field, the induced voltage in the sense windings will be symmetrical, i.e., contain only odd harmonics of the fundamental driving current that produced the applied field. In the presence of an external field, the induced voltage becomes asymmetrical, the asymmetry and the corresponding even harmonics being proportional to the amplitude of the component of the external field parallel to the axis of the core.

The fluxgate magnetometer has been used widely in various applications where sensitivity, stability, and absolute accuracy has been sacrificed for the features of simplicity, low cost, low power, and ruggedness. Since it is a directional device, measuring only the component parallel to the axis of the core, a triaxial arrangement of three cores is necessary for total field measurements.

B. OPTICALLY PUMPED RESONANCE

The optically pumped resonance magnetometers (chiefly Rubidium, Cesium, and Helium) measure the total intensity of the magnetic field by an extremely accurate detection of the Zeeman effect. Due to the Zeeman effect the energy levels associated with a valence electron become split into sublevels whose separations are dependent on the total

intensity of the magnetic field. The detection of this splitting is based on the principles of optical pumping and monitoring. Optical pumping is described in a tutorial manner in Reference 4 and for the Cesium atom in Appendix A.

Figure 3.1 shows a simplified block diagram of a typical pumping apparatus. A light source producing an intense collimated beam of light is first filtered and circularly polarized and then passed through a resonance cell containing the vapor to be pumped. As the light is absorbed and emitted by the sample atoms, optical pumping proceeds and results in a steady state non-equilibrium population distribution over the magnetic states of one of the ground levels. In this pumped condition the sample is prepared for resonance

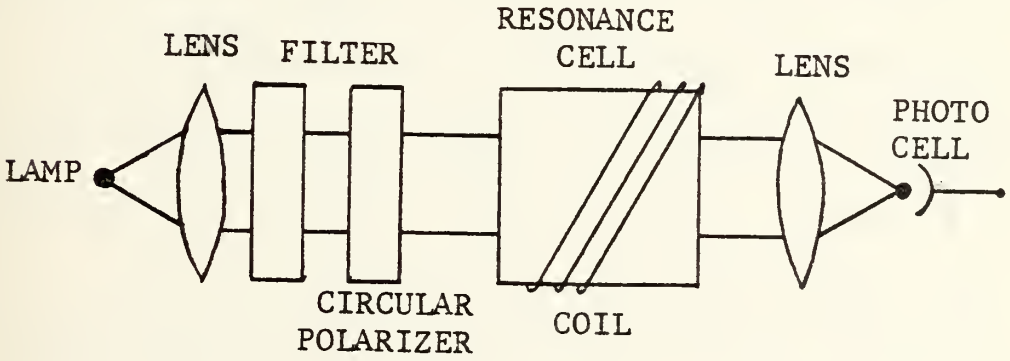

Figure 3.1 Typical Pumping Apparatus

and is characterized by a net magnetization $M = M_z$ along the ambient magnetic field direction. Resonance transitions between the Zeeman states of the pumped level are induced by subjecting the sample to an RF field of frequency f_1 sufficiently close to the resonant frequency f_0 and with component H_1 perpendicular to the ambient field $H_0 = H_z$. The RF drive field introduces Zeeman coherence, and according to Bloch's equations the steady state behavior of the magnetization M changes and is no longer parallel to H_0 but now has a transverse component $M_\perp$ precessing around H_0 at the frequency of H_1. Consequently the M_z component along H_0 decreases, and the light transmission also. This variation of light intensity with the applied RF, being a maximum at resonance, can be used as a detection method, or the photocell can be made to observe the signal corresponding to the M_x component, which is precessing or rotating at the same RF applied which induced the resonance. The photocell output is then at the resonant frequency. Appendix B details the two detection systems commonly used. The resonant frequency is proportional through a constant to the magnetic field (4.66 Hz/gamma for Rb; 3.499 Hz/gamma for Cs; 28 Hz/gamma for He) and thus the field measurement.

Figures 2.4 through 2.10 were all recorded using an optically pumped magnetometer and the appearance of the micropulsations differ somewhat from those one would find in a reference handbook. This illustrates an undesirable feature of this magnetometer when used in micropulsation work. It is equally sensitive to all frequencies and the larger amplitude, lower frequency changes such as the diurnal variation continually drive the highly sensitive instrument offscale. The result is a sloping and discontinuous output that is difficult to interpret.

C. CRYOGENIC SQUID

A cryogenic SQUID (Superconducting Quantum Interference Device) magnetometer consists of three basic parts: 1) a superconducting ring embodying a Josephson junction; 2) an externally generated HF field used to provide a small field variation superimposed on the ambient dc field and therefore to control the amount of flux through the ring; 3) an electronic detection system to observe the impedance of the coil and make the output response a linear function of the ambient field.

The operation utilizes the principle that if the flux through the ring is varied on either side of a minimum or

maximum energy value, associated with the Josephson coupling energy, the SQUID will generate a field which will respectively oppose or add to the variation. The energy contribution of the SQUID aiding or opposing the applied field variation according to whether the ambient dc field amounts to a minimum or maximum energy value constitutes a parametric control of the inductance measured at the coil terminals. In other words, the SQUID alternately behaves diamagnetically and paramagnetically and will decrease and increase the inductive reactance.

Through the use of a detector to monitor the coil impedance one can observe the variation of impedance with ambient magnetic field. Because the impedance variation is periodic a phase locked feedback loop is normally included to obtain a response linearly related to the field.

Because SQUID compares the energy values of the ambient and weak superimposed fields, it measures only a change in field, not the total intensity.

D. GRADIOMETER

A gradiometer, in theory, would measure the space gradients of the magnetic field, that is:

$$\frac{\partial X}{\partial x}, \frac{\partial X}{\partial y}, \frac{\partial X}{\partial z}$$

$$\frac{\partial Y}{\partial x}, \frac{\partial Y}{\partial y}, \frac{\partial Y}{\partial z}$$

$$\frac{\partial Z}{\partial x}, \frac{\partial Z}{\partial y}, \frac{\partial Z}{\partial z}$$

Only five of these are independent because X, Y, and Z are the derivatives of a potential and because of Laplace's equation. In practice gradiometers are constructed by taking the finite difference of two magnetometers, therefore cancelling the ambient field that is approximately equal at both sensors. A local change or anomaly that is closer to one of the two sensors is not cancelled and therefore recorded.

The disadvantage of the gradiometer is that with respect to a single sensor magnetometer most magnetic anomalies fall off as the inverse cube, $1/r^3$ where r is the distance from the anomaly to the sensor, but the gradiometer anomaly falls off as the inverse fourth power, $1/r^4$ where r is the

distance from the anomaly to the center of the sensor configuration.

In Reference 10, Langan, Lynch, and Slack reported a gradiometer used in geophysical prospecting that measured the vertical gradient $\Delta H/\Delta z$ where H was the magnitude of the anomaly and z the distance to the anomaly. It was constructed of two optically pumped sensors vertically separated and towed by a helicopter.

Both the optically pumped and SQUID magnetometers are easily converted to gradiometers because of the form of their output, but they will measure different gradients. The optically pumped gradiometer, constructed of total field magnetometer sensors will measure the total field gradient $\Delta F/\Delta z$. A SQUID gradiometer, constructed of devices sensitive only to a field change will measure a field component gradient $\Delta Z/\Delta z$, for example.

TYPE	RESOLUTION (GAMMA)	MEASURE-MENT	FREQUENCY RESPONSE	COST	ADVANTAGE	DIS-ADVANTAGE	GRAD-IOMETER
PROTON PRECESSION	10^{-2}	TOTAL FIELD INTENSITY	1 Hz	MOD	ACCURATE RUGGED	DISCONTIN-UOUS MEASURE-MENT	DIFFI-CULT
OPTICALLY PUMPED ALKALI	10^{-3}	TOTAL FIELD INTENSITY	100 Hz	HIGH	SENSITIVITY	ORIENTA-TION EFFECTS	EASY
OPTICALLY PUMPED HELIUM	10^{-3}	TOTAL FIELD INTENSITY	100 Hz	VERY HIGH	SUITABLE FOR MOBILE USE	COST	EASY
FLUXGATE	10^{-2}	COMPONENT OF THE FIELD	10 Hz	LOW	SIMPLE	SENSITIV-ITY	EASY
SQUID	10^{-5}	CHANGE IN FIELD	1000 Hz	HIGH	SENSITIVITY	TEMPERA-TURE CONTROL	VERY EASY

Table 1 Comparison of Magnetometers

IV. SYSTEM DESCRIPTION

The overall system can be broken into three subsystems: 1) the data collection subsystem; 2) the periodmeter and interface subsystem; 3) the processing and display subsystem.

A. DATA COLLECTION SUBSYSTEM

The magnetometer used was the Varian V-4938 Cesium system. It used an optically pumped cesium sensor of the auto-oscillating type. A block diagram of the Varian system is shown in Figure 4.1.

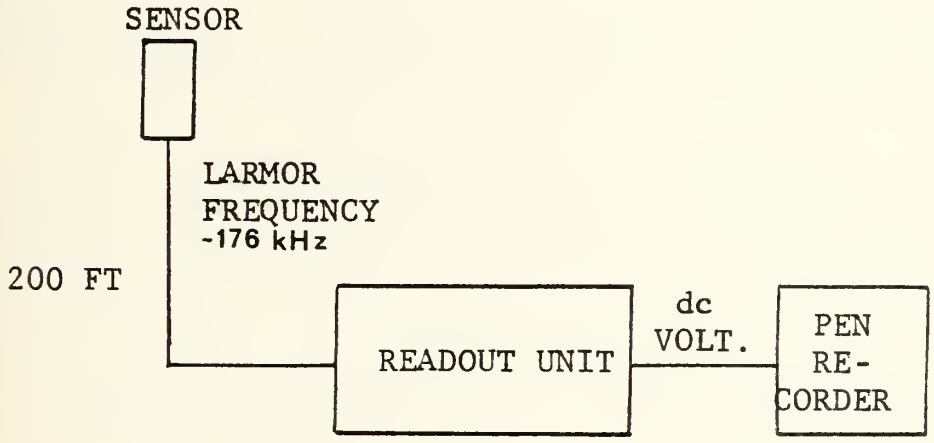

Figure 4.1 Varian Magnetometer

The sensor head produces the RF signal (Larmor frequency) directly proportional to the total magnetic field intensity. This signal together with the input power for the sensor is conducted along a 200 foot coaxial cable to the main readout

unit. The readout unit converts the Larmor frequency to a highly stable dc voltage which drives the pen recorder. The system was located in a wooded area approximately one mile from the Naval Postgraduate School, which provided a near noise free environment.

A more complete block diagram of the V-4938 system is shown in Figure 4.2. The RF Larmor frequency, which was approximately 176 kHz, from the sensor is mixed in the read-out unit to the 100 Hz to 3 kHz range and then applied to a highly stable frequency to voltage converter. This dc voltage, which now represents the field value, is passed through biasing circuitry to interface it to the pen recorder.

The system configuration used for data collection differed from the Varian recommended system of Figure 4.2. This was necessary because of the requirement to record the output on magnetic tape. The actual system used is shown in Figure 4.3. This configuration was used because the mixer output of the readout unit was a square wave and its frequency content exceeded the 5 KHz range of the tape recorder. The coupler unit shown connects between the readout unit and the sensor to provide dc power to the sensor and it also contains a mixer, but its output is a sinusoid rather than a square wave and recorded nicely. The coupler units primary

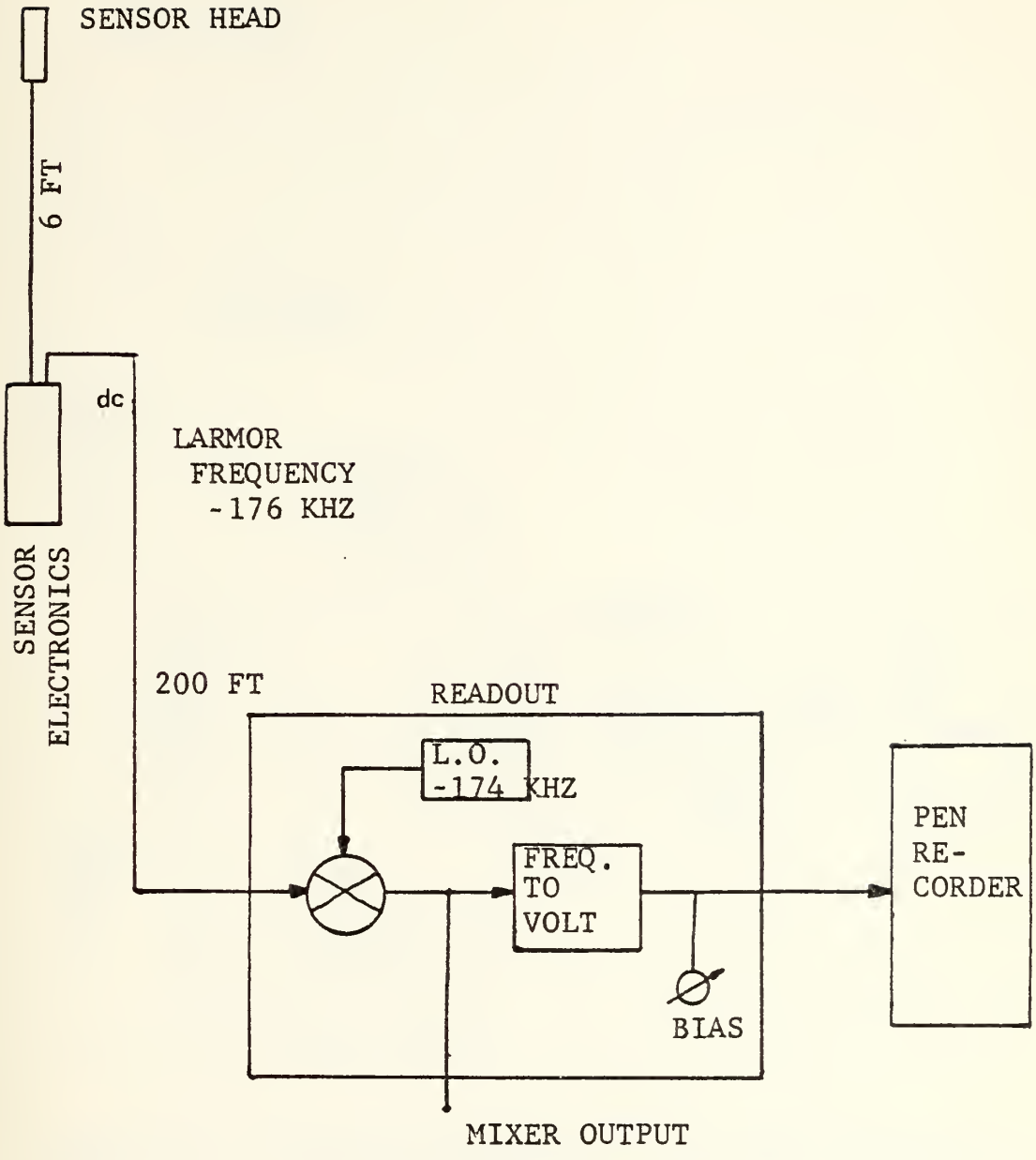

Figure 4.2 Magnetometer Signal Flow

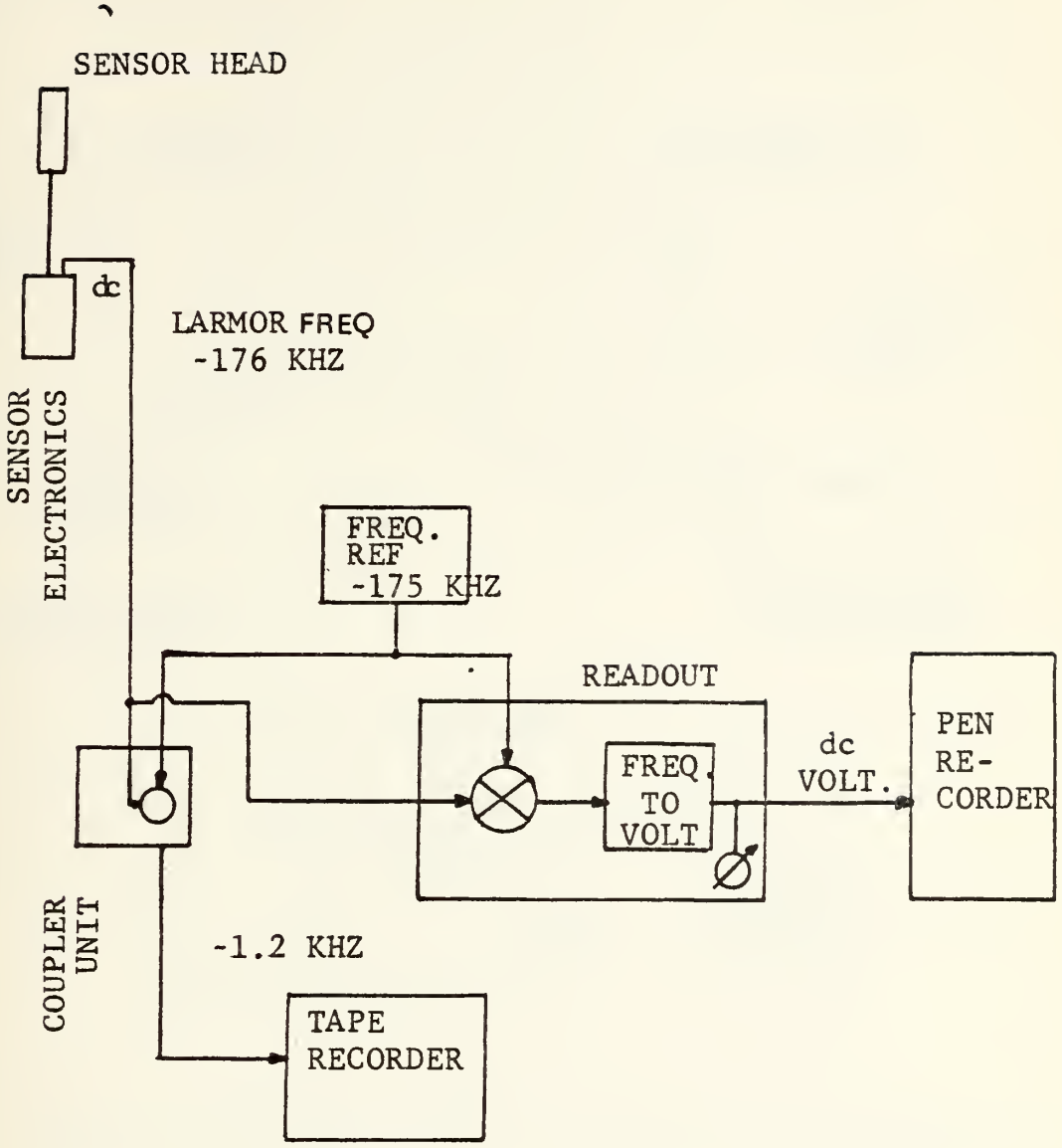

Figure 4.3 Magnetometer Data Collection Configuration

purpose is to convert the system to a gradiometer which is shown in Figure 4.4.

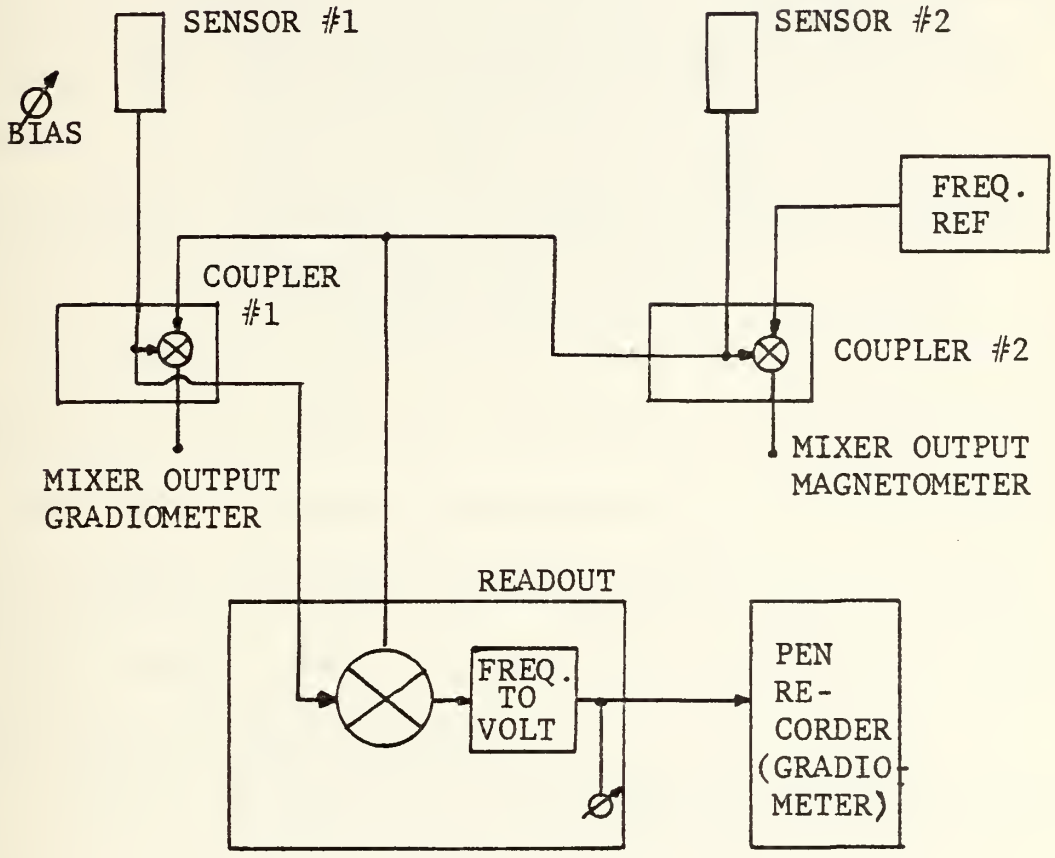

Figure 4.4 Gradiometer Data Collection Configuration

Again this is not the configuration recommended but this provided both a magnetometer and gradiometer output suitable for recording and still allowed the pen recorder to monitor the gradiometer signal. The bias applied to the one sensor was required to generate a difference

frequency between the sensors sufficient to drive the mixer circuitry. The sensors were located approximately 180 ft apart resulting in a Larmor frequency difference of only approximately 30 Hz, and the mixers required a difference of at least 100 Hz and optimally between 1 and 3 kHz. Figure 4.5 shows the readout units mixer output with an insufficient difference frequency and Figure 4.6 shows the coupler units sinusoidal mixer output.

One other system characteristic imposed a limitation, that was the orientation sensitivity of the single cell sensor. For optimum performance the sensor head needed to be oriented both toward magnetic North and 45° to the total field vector. Figure 4.7 shows the non-metallic housing and Figure 4.8 the geometry.

Figure 4.9 shows the system components and equipment used to monitor and record the data.

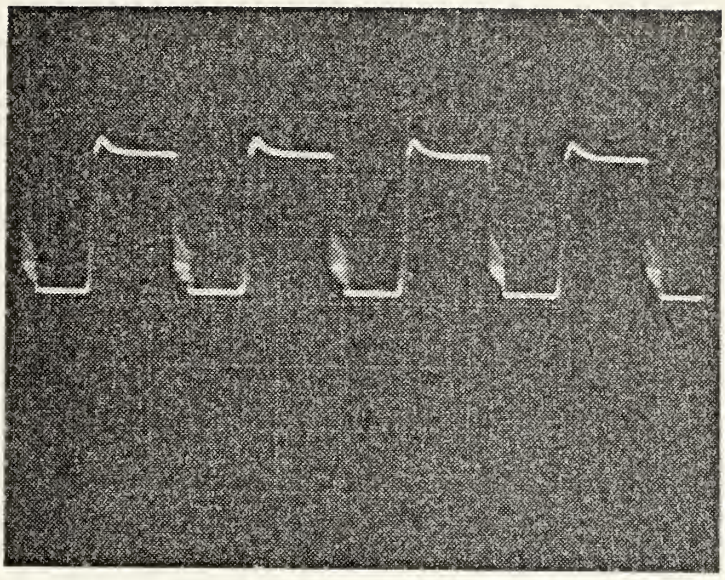

Figure 4.5 Distorted Readout Unit Mixer Output

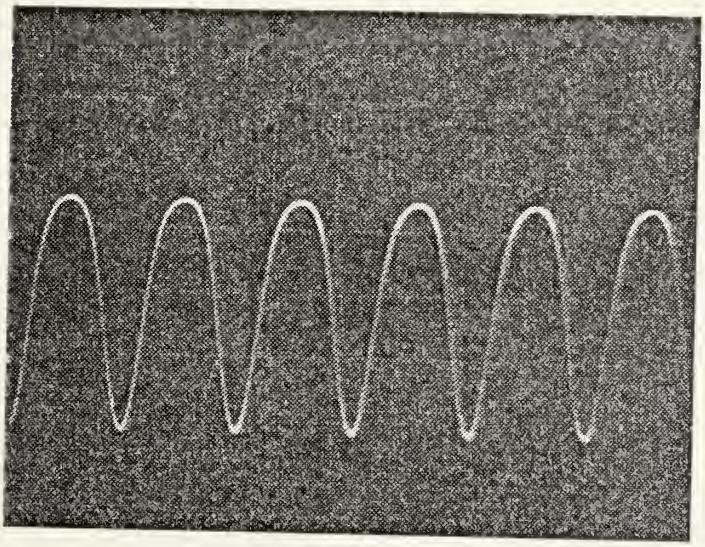

Figure 4.6 Coupler Unit Mixer Output

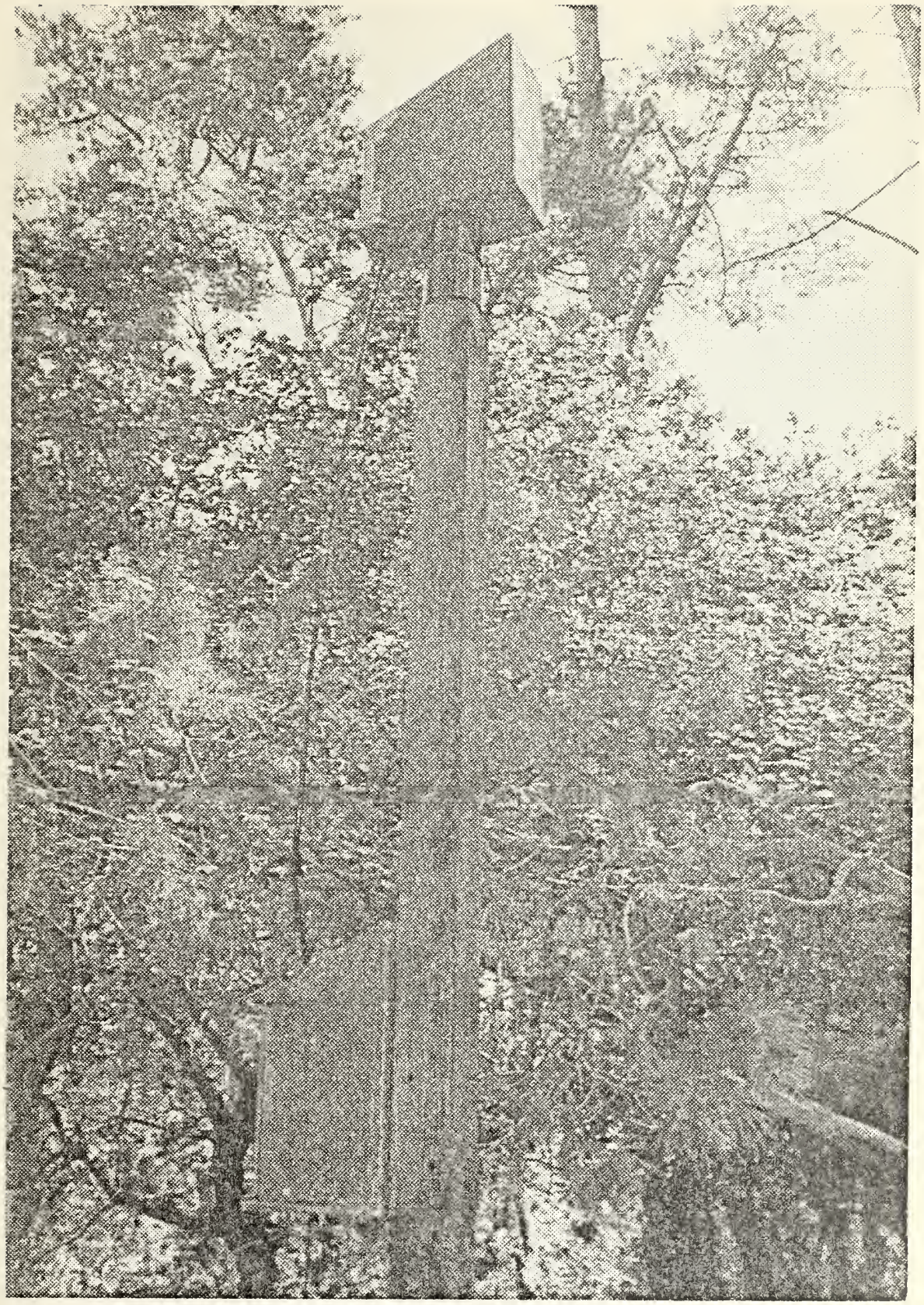

Figure 4.7 Non-Metallic Housing Used to Fulfill Orientation Requirements

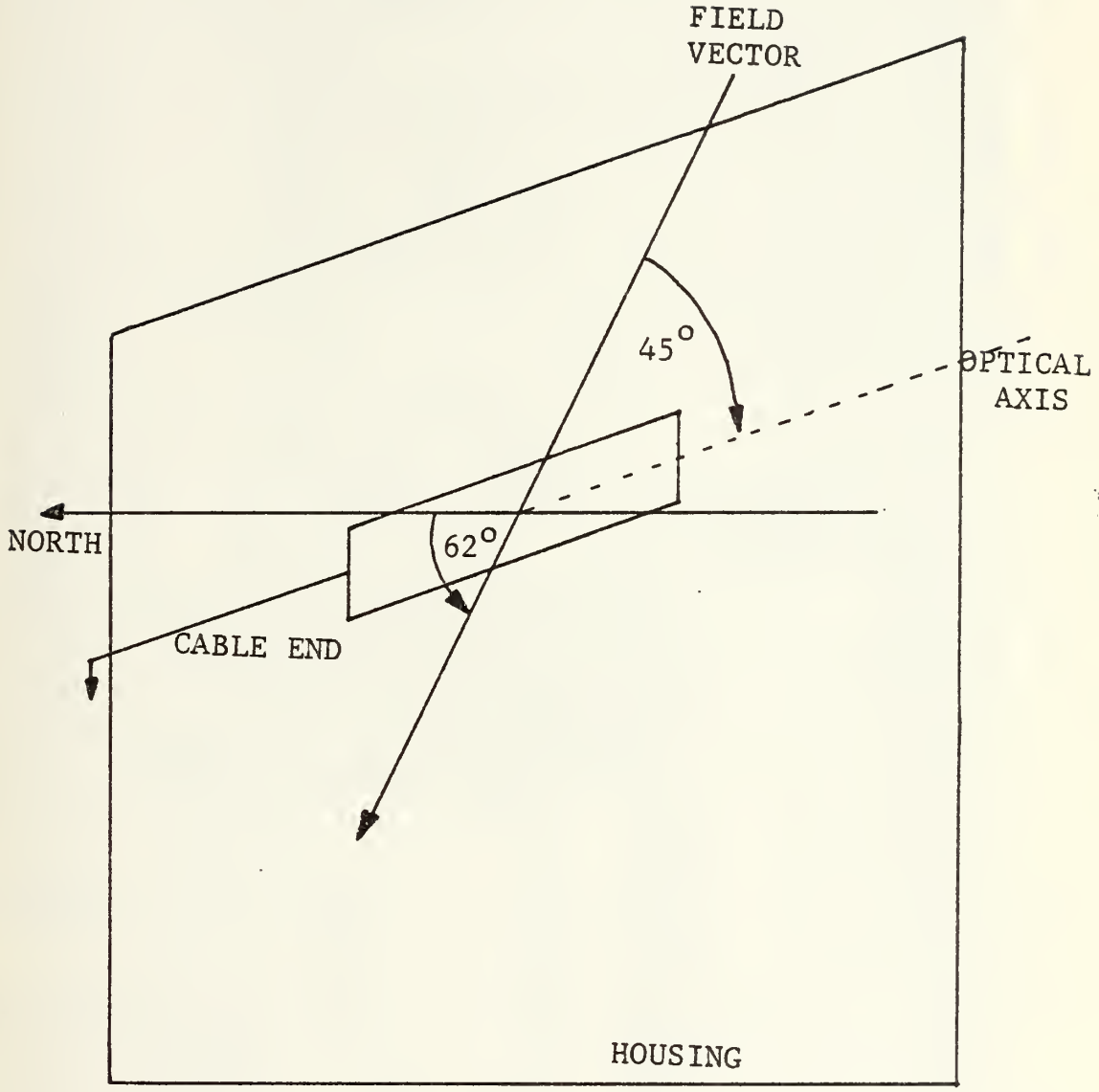

Figure 4.8 Sensor Housing Geometry

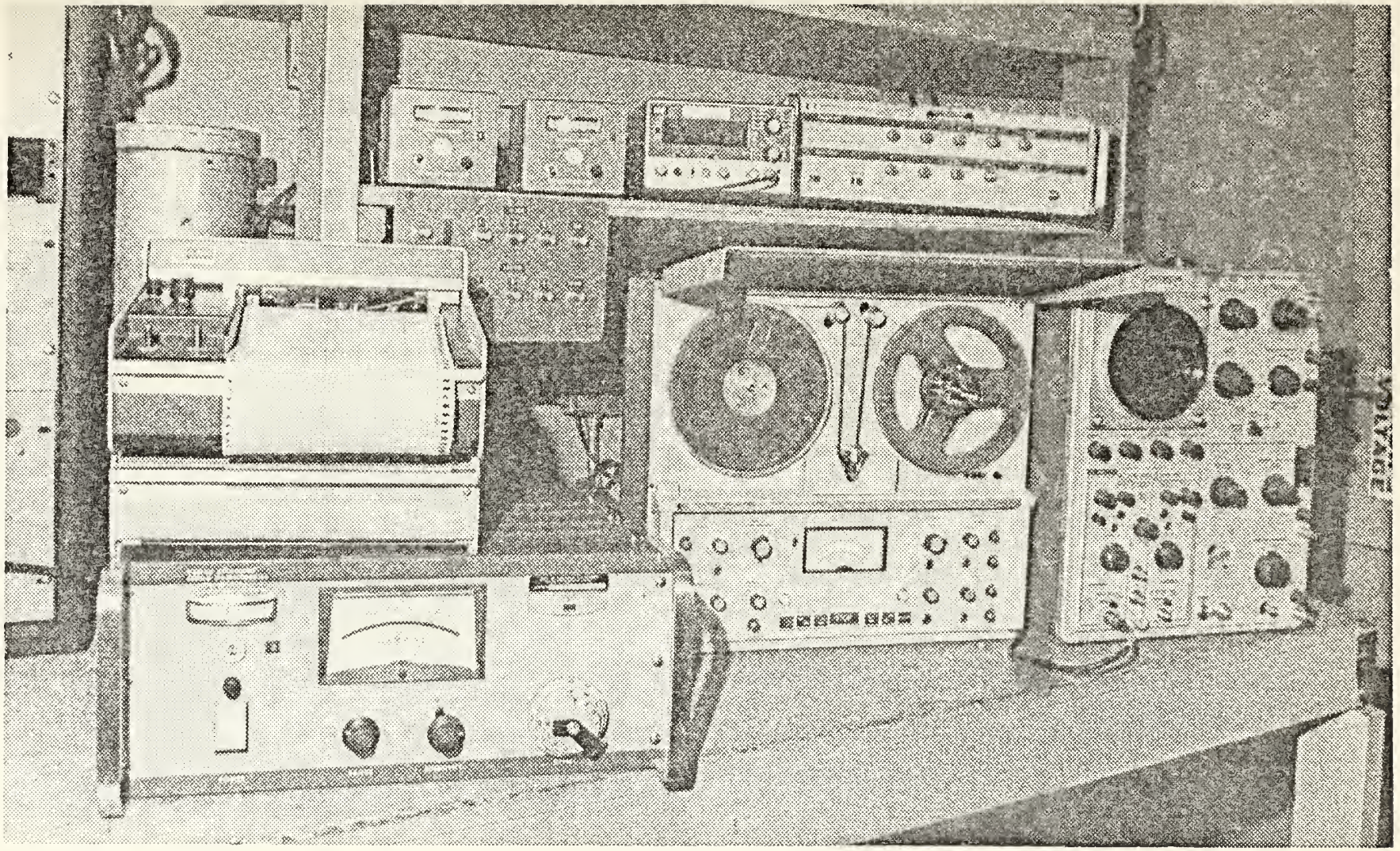

Figure 4.9 Equipment Setup in Monitoring Shack. Shows Readout Unit, Pen Recorder, Coupler Units, and Tape Recorder

B. PERIODMETER AND INTERFACE SUBSYSTEM

The frequency response of the magnetometer when used with the readout unit is limited to 20 Hz by the discriminator and even more by the pen recorder response. The theoretical frequency response of the sensor is limited only by the bandwidths of the amplifier and feedback loop, which are extremely wide. To take advantage of this the mixer output was recorded on an HP-3960 FM tape recorder. This signal still contained the high frequency components present in the Larmor signal. A periodmeter and interface unit were constructed to measure the period of successive cycles and interface this digital count into the XDS-9300 computer, for further display on the AGT-10 graphics console.

Figure 4.10 is a block diagram of the periodmeter. The data signal is passed through a simple RC high pass filter to reject any 60 Hz modulation that might be present and then input to a zero crossing detector. The falling edge of this is used to trigger a one-shot that inhibits the otherwise free running 4 MHz count. The one-shot pulse is inverted and delayed and the rising edge used to trigger flip flop type memories. Once the count is latched another one shot is used to clear the count and provide a signal

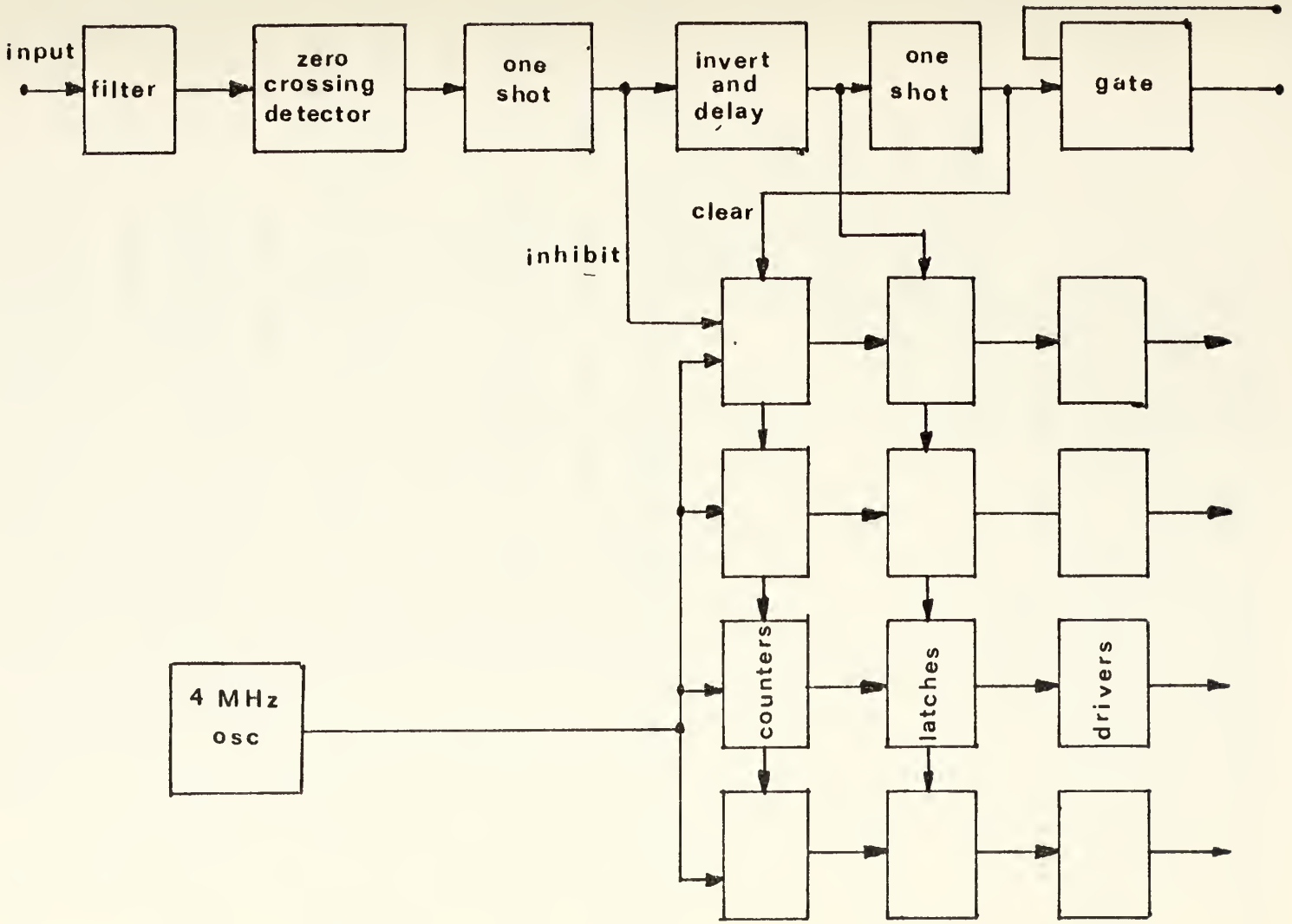

Fig 4.10 PERIODMETER

indicating the cycles completion. The cycle then repeats. The actual circuits and timing diagrams are presented in Appendix C.

A direct access channel into the XDS-9300 was used to input the binary count directly into sequential memory locations. Figure 4.11 is a block diagram of the periodmeter and interface. To implement the input the following sequence of instructions were used:

```
EOM  032400
SKS  032400
BRU  $-1
PIN  ITEM
```

With the execution of the EOM instruction the contents of the control register are available at the output connector. This is decoded and toggles a flip flop to alert the periodmeter that the XDS is ready to accept an input. This EOM alert and the periodmeter's completion signal are logically combined and send a ready signal to the XDS-9300. Upon receipt of this ready signal and the execution of the PIN the data is transferred and stored in the location specified in the PIN instruction. The SKS instruction is used to sense if both the computer and periodmeter are ready. If both the EOM alert and completion signal are not present, the next

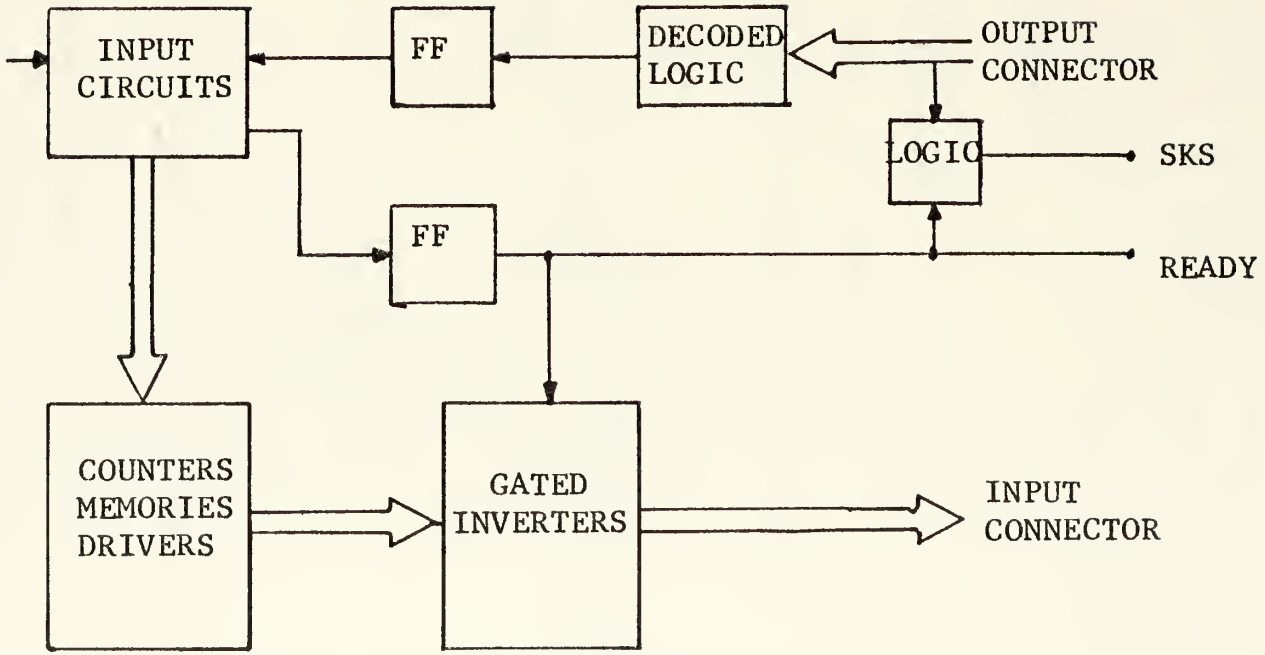

Figure 4.11 Periodmeter and Interface Block Diagram

instruction, branch unconditionally back to the SKS, is executed. This looping continues until both systems are ready. If both are ready the branch instruction is skipped. The ready signal is also used to gate the data through inverters because it is inverted prior to being transferred into the XDS-9300. The actual circuit diagrams are presented in Appendix C.

C. DISPLAY SUBSYSTEM

A block diagram of the data flow in the interface and display subsystems is shown in Figure 4.12.

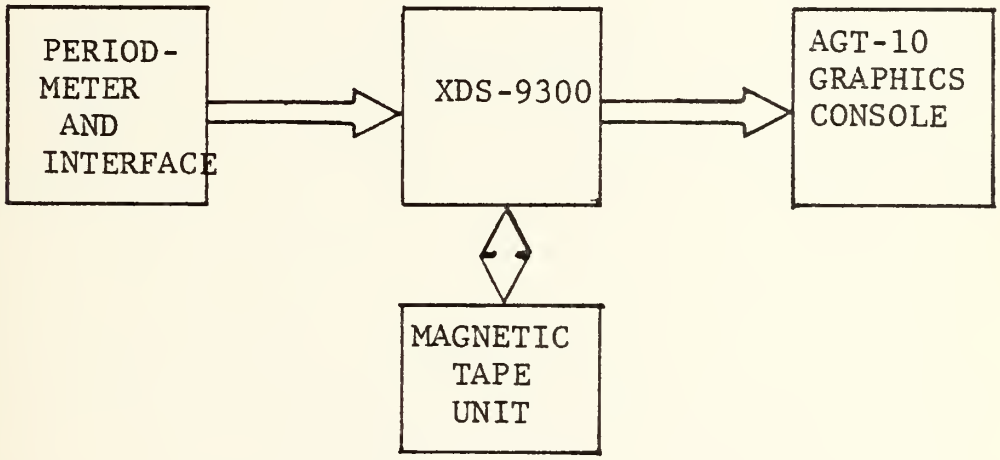

Figure 4.12 Data Flow From Periodmeter Through Display

The physical block length of data input to the XDS-9300 was 12,288 points. A mean and standard deviation of these points was found and values not within five standard deviations were discarded. This eliminated erroneous data

points caused by noise spikes either in the computer, periodmeter, or on the recording. The block was then buffered out in groups of 4096 points and written on magnetic tape. To be displayed the data was buffered back in, again in groups of 4096 points, normalized, and displayed on the AGT-10 graphics console. Both programs are self-explanatory and are presented in Appendix D. Signal flow diagrams for the two are shown in Figure 4.13 and 4.14.

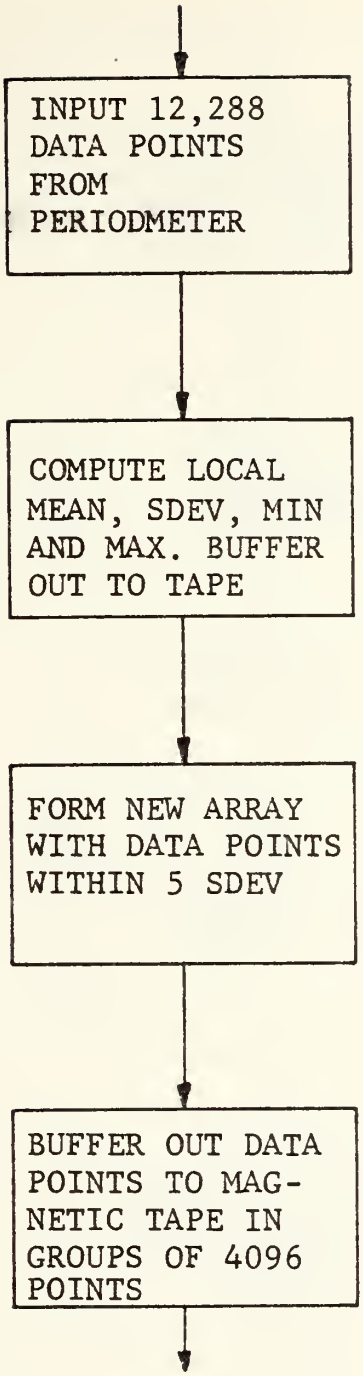

Figure 4.13 Signal Flow Diagram of Input Program

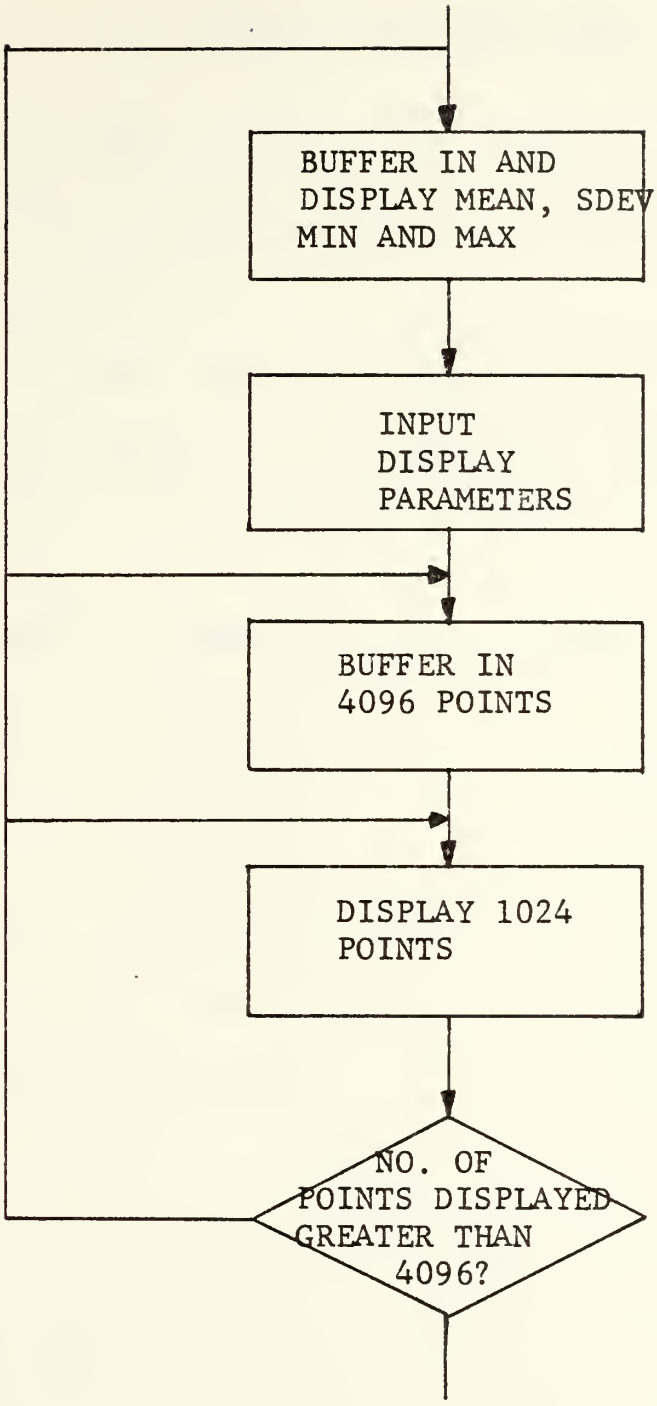

Figure 4.14 Signal Flow Diagram of Display Program

V. RESULTS AND CONCLUSIONS

The system was tested in three phases: 1) laboratory signals; 2) tape recorded laboratory signals; 3) magnetometer signals.

First, constant frequency signals from a laboratory generator were applied. The frequencies sampled and the resulting period measurement are listed in Table 2.

FREQUENCY Hz	MEAN PERIOD μsec	THEORETICAL PERIOD μsec
1000.0	999.25	1000.00
1000.1	999.00	999.00
1000.5	998.75	999.50
1001.0	998.25	999.00
1003.0	996.25	997.01
1005.0	994.25	995.02

Table 2

The .75 μsec difference between theoretical and actual is due to the clear and latch time of the periodmeter. These measurements were within ±1 count or ±25 μsec with a 4MHz time base. This established the resolution of the device as .1 Hz or better. The outputs displayed for the sampled

frequencies of 1000.0 Hz, 1000.1 Hz, and 1001.0 Hz are shown in Figures 5.1 - 5.3 and a distinguishable difference is noticeable. To insure the system would follow a rapidly changing frequency a swept frequency signal was applied and the display shown in Figure 5.4.

The second phase of testing was designed to determine the magnitude of the tape recorder flutter and noise. It involved recording the same frequencies used in phase 1 and comparing the results. The frequencies, mean period measurement, and standard deviation for each are listed in Table 3.

FREQUENCY Hz	MEAN PERIOD μsec	STANDARD DEVIATION μsec
1000.0	999.25	.575
1000.1	999.00	.700
1000.5	998.75	.850
1001.0	998.25	.550
1003.0	996.25	.650
1005.0	994.25	.675

The mean period, calculated for 12,288 periods, remained the same. The average standard deviation was .667 μsec. This established the RMS noise level of the system when operated in the 1200 Hz range to be approximately 1 Hz or

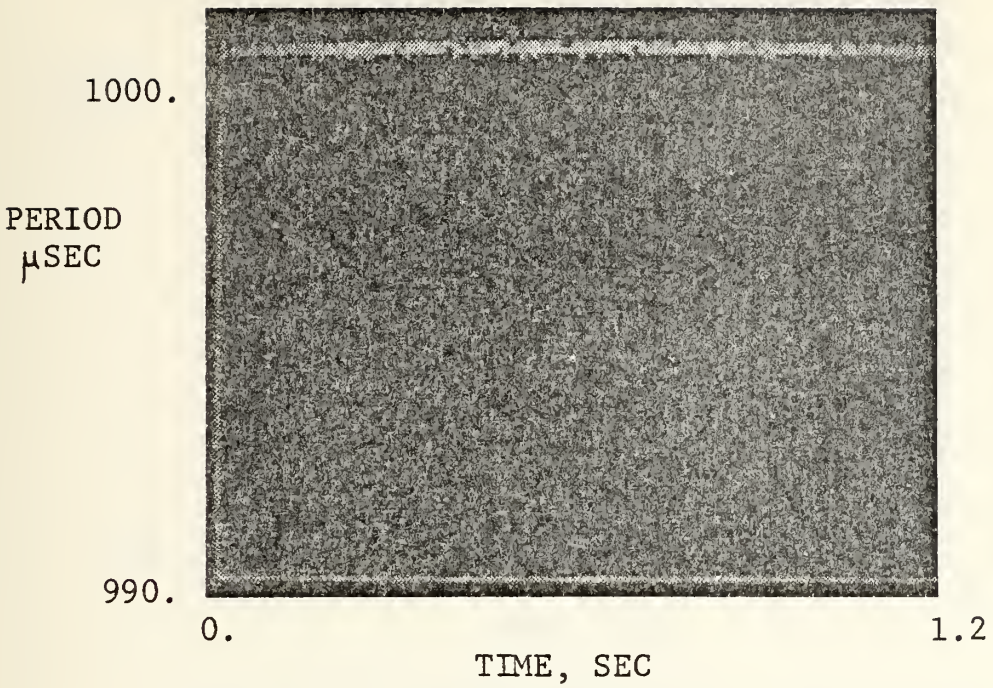

Figure 5.1 Output Display of Direct Input 1000.0 Hz Laboratory Signal

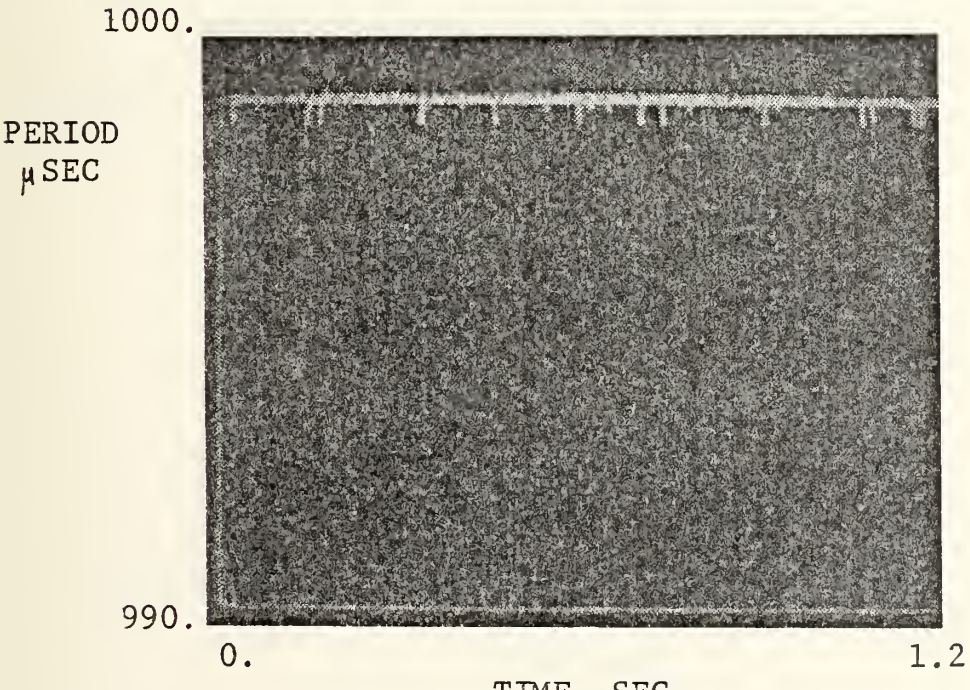

Figure 5.2 Output Display of Direct Input 1000.1 Hz Laboratory Signal

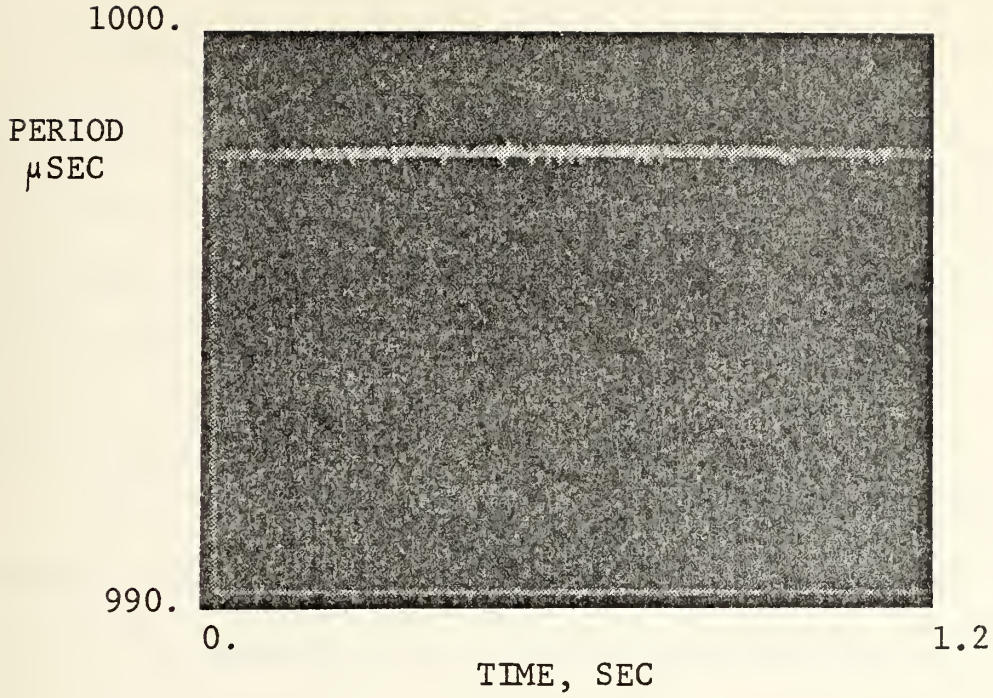

Figure 5.3 Output Display of Direct Input 1001.0 Hz Laboratory Signal

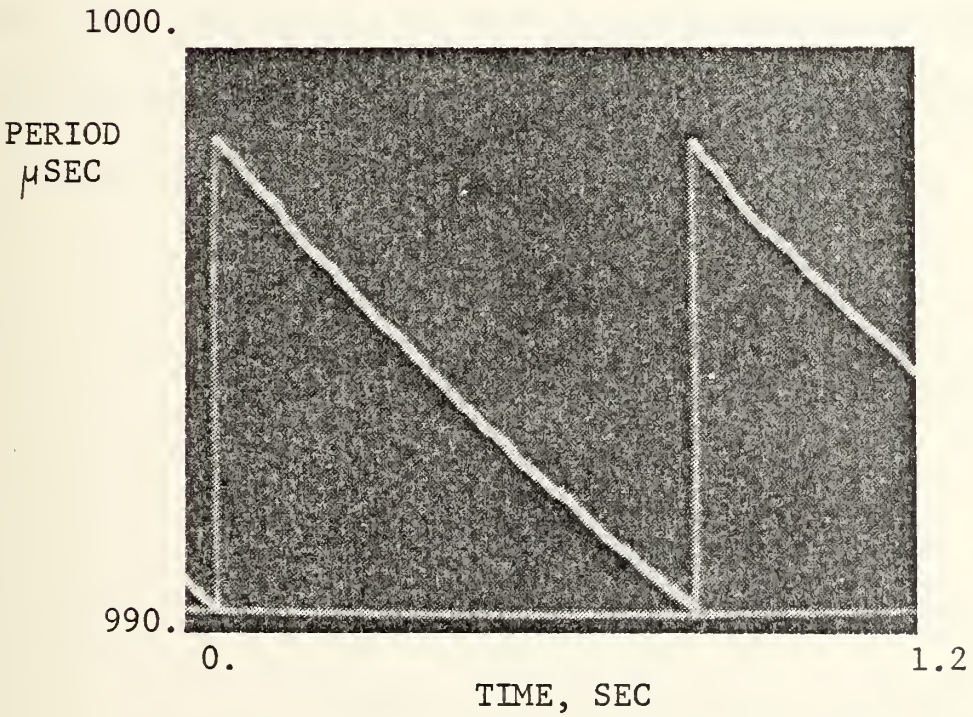

Figure 5.4 Output Display of Direct Swept Frequency Laboratory Signal

.27 gamma. The AGT-10 displays for the sampled frequencies of 1000.0 Hz and 1000.1 Hz are shown in Figures 5.5 and 5.6. The previously discernible difference is now buried in tape recorder noise. Figure 5.7 shows the frequency transition from 1001.0 to 1003.0 Hz and this 2 Hz difference is easily distinguishable.

The final phase of testing involved introducing a known magnetic disturbance and analyzing the magnetometer output. A 72 turn Helmholtz coil, in the configuration of Figure 5.8, was used to introduce the disturbance. The sensor was placed on the axis of the coil and the coil aligned with the total field vector. This insured the induced field of the coil would directly aid or oppose the ambient field and allowed changes of predetermined amounts. With the simplified geometry

$$H = \frac{N\ I\ R^2}{2\ r^3} \qquad \frac{4\pi}{10^{-2}}$$

where N = number of turns in the coil

I = current in the coil

R = radius of the coil

r = distance from coil to sensor

$\frac{4\pi}{10^{-2}}$ was required for conversion from ampere-turns per meter to gammas.

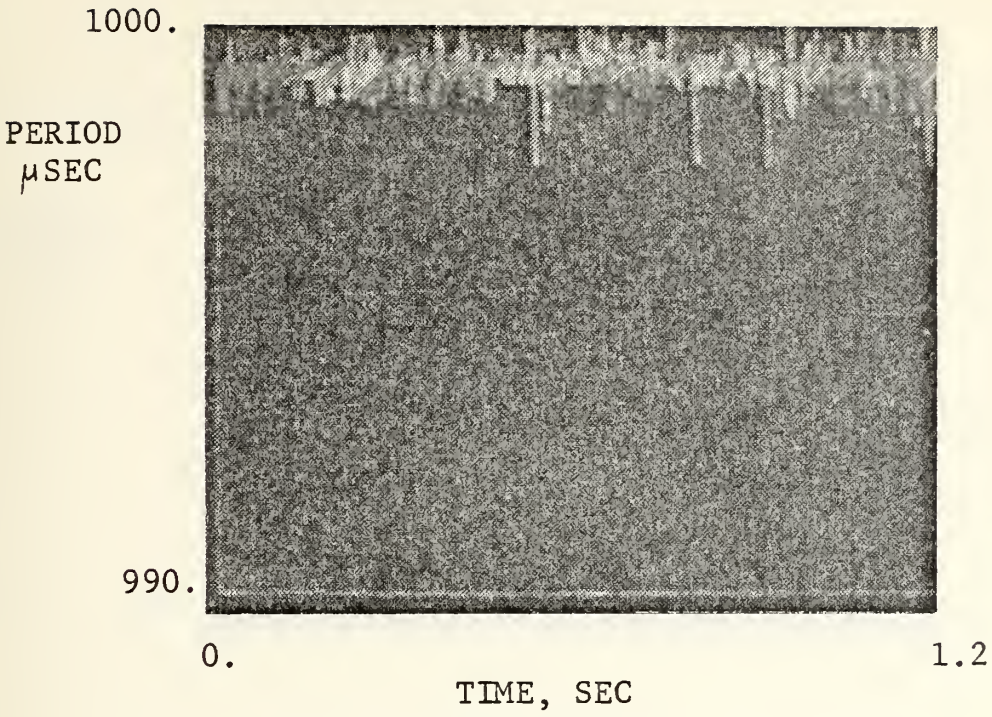

Figure 5.5 Output Display of Recorded 1000.0 Hz Laboratory Signal

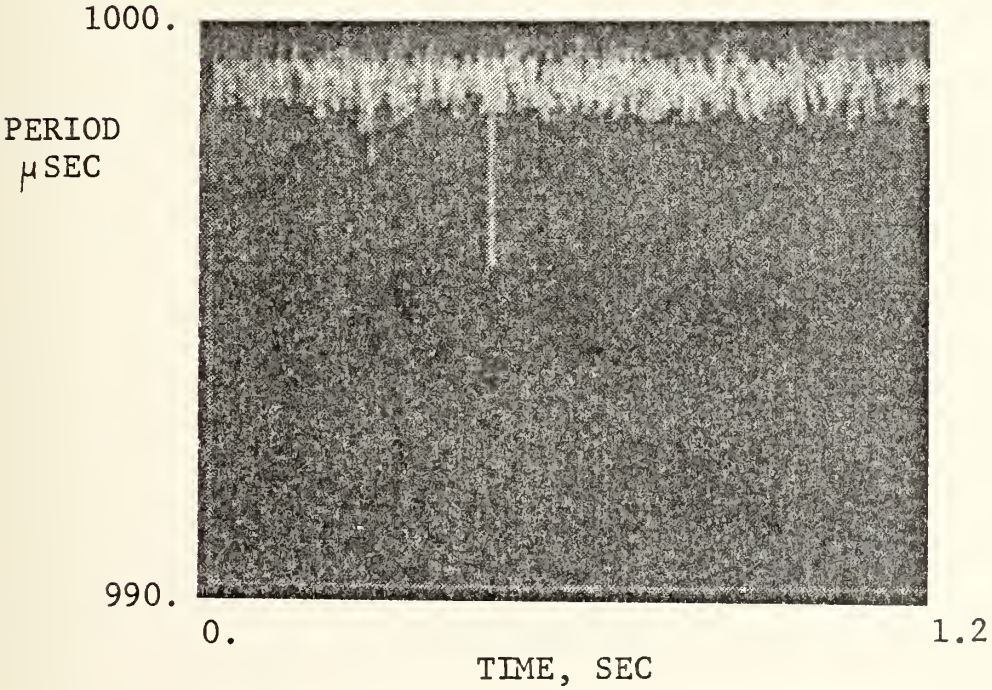

Figure 5.6 Output Display of Recorded 1000.1 Hz Laboratory Signal

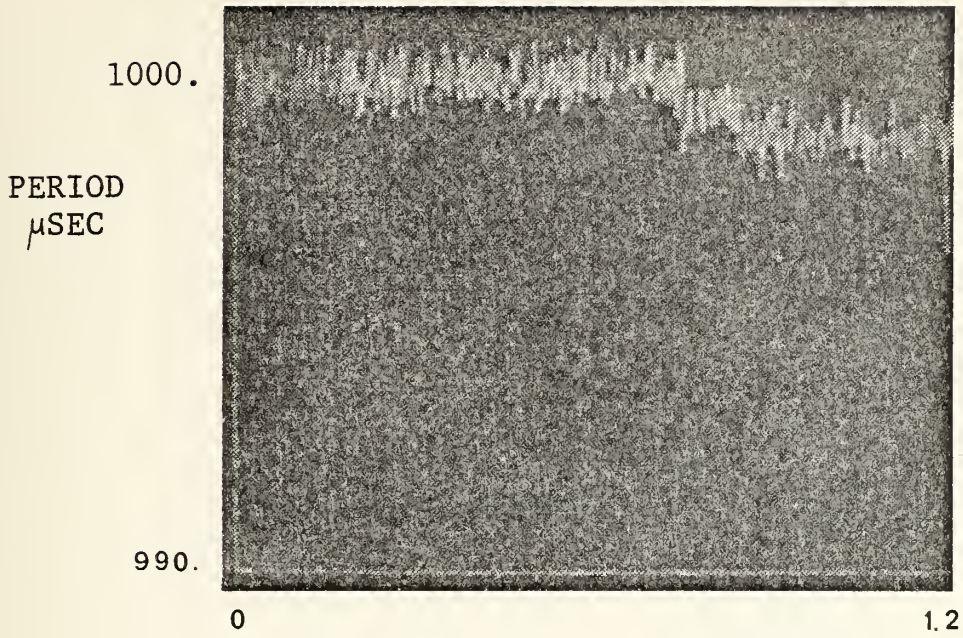

Figure 5.7 Output Display of Recorded1001.0 and 1003.0 Hz Laboratory Signal

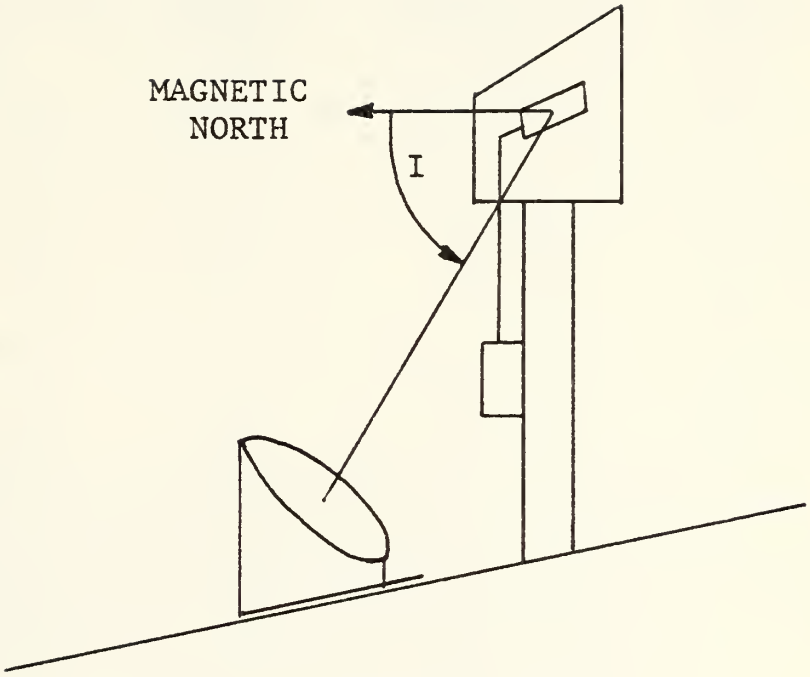

Figure 5.8 Coil and Sensor Geometry Used to Disturb the Field

The coil utilized had a mean radius of 33 cm and was placed 3.5 m from the sensor. Table 4 tabulates the various currents and observed versus predicted changes. Figures 5.9 through 5.30 show the magnetometer pen recorder output and a selected time frame of the corresponding AGT-10 display.

I ma	THEORETICAL ΔH	MAGNET. ΔH	THEORETICAL Δf	DISPLAY Δf
400	45.964	46.0	160.874	160.893
300	34.473	35.0	120.655	120.666
240	27.578	27.5	96.524	96.531
200	22.982	22.7	80.437	80.442
160	18.386	18.7	64.350	64.354
120	13.789	13.8	48.262	48.264
100	11.491	11.1	40.218	40.219
90	10.342	9.6	36.197	36.198
80	9.193	9.0	32.175	31.176
70	8.044	8.4	28.153	28.154
60	6.895	6.8	24.131	24.132
40	4.596	4.2	16.087	16.086
20	2.298	2.1	8.044	8.045
10	1.149	1.1	4.022	4.023
5	.574	.65	2.011	2.012

Table 4

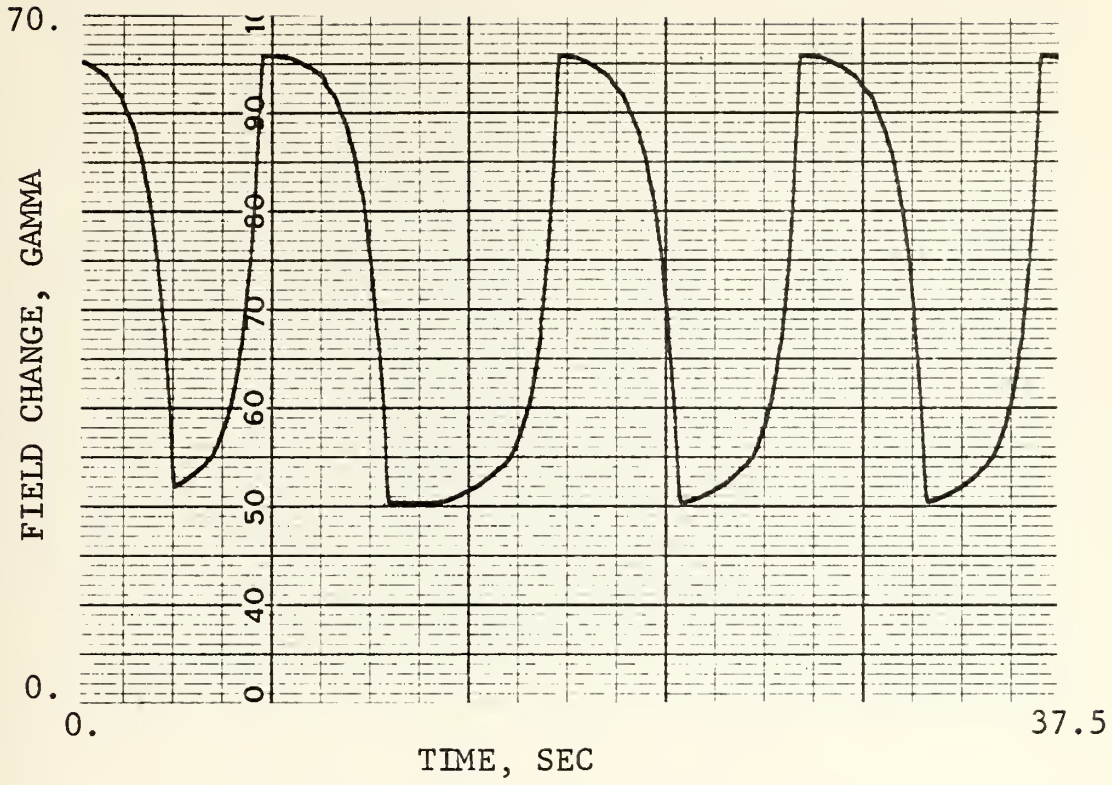

Figure 5.9 Pen Recorder Output for ΔH= 45 gamma

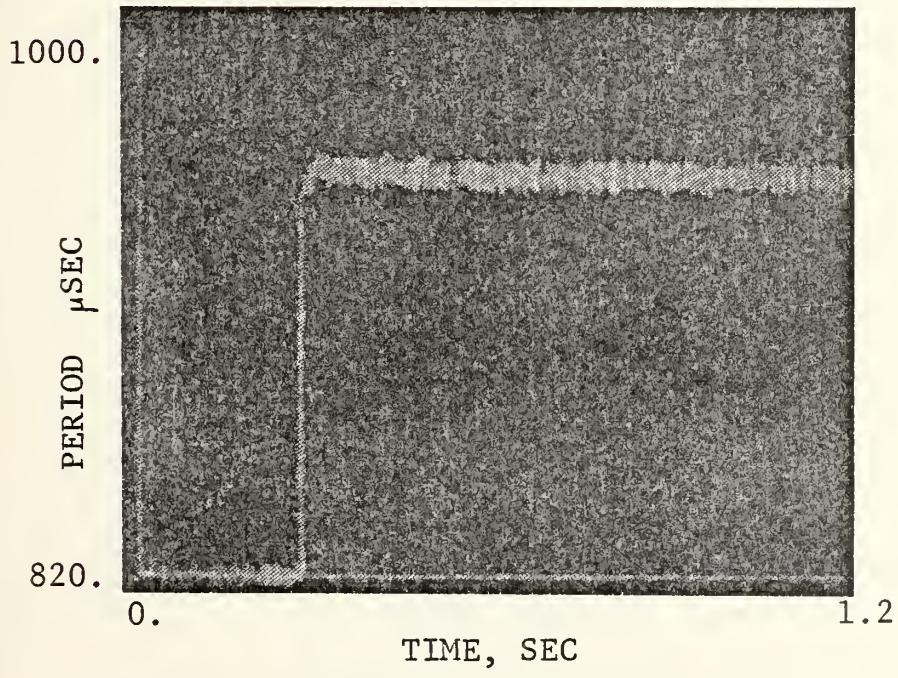

Figure 5.10 AGT-10 Display for ΔH= 45 gamma

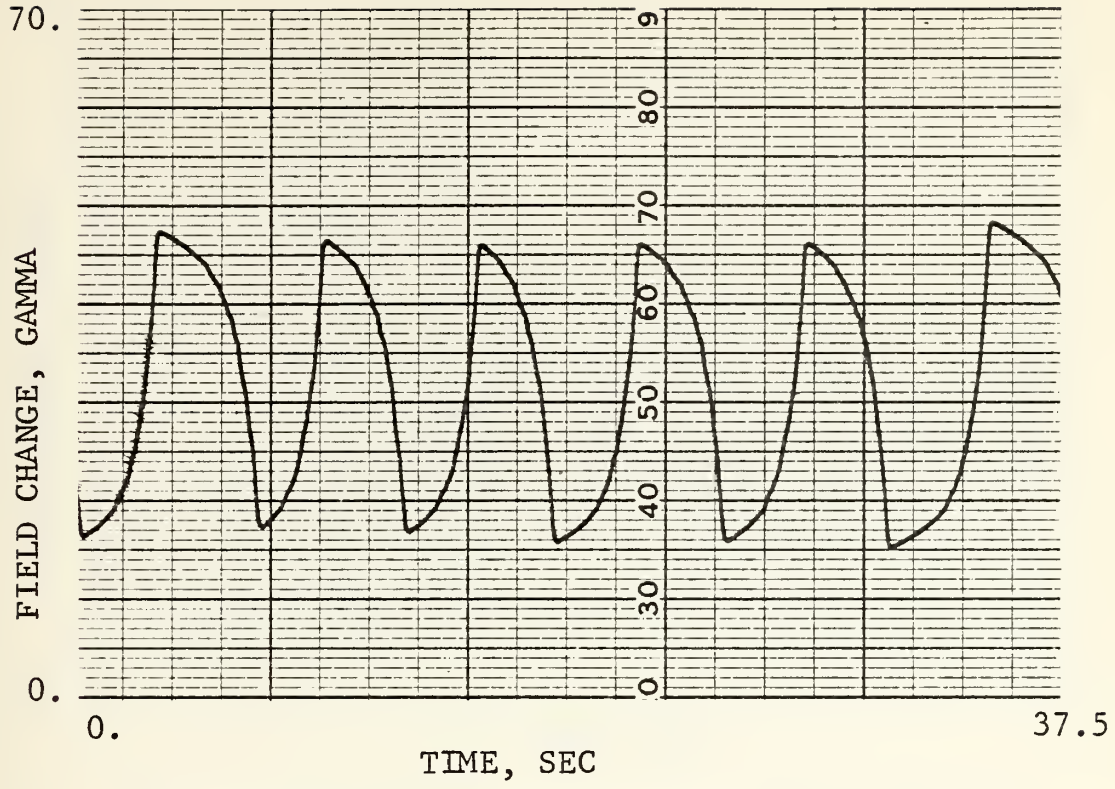

Figure 5.11 Pen Recorder Output for ΔH= 35 gamma

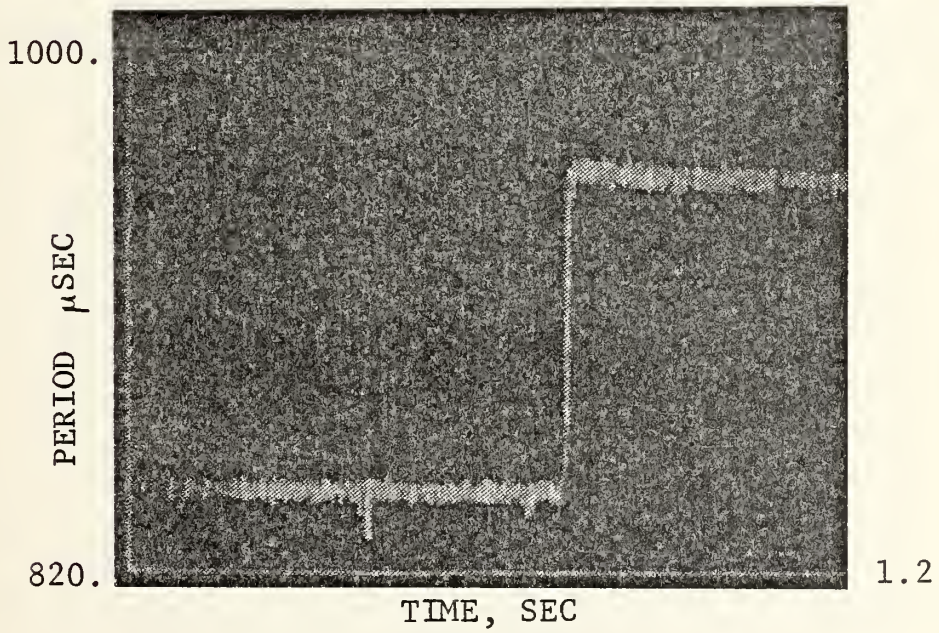

Figure 5.12 AGT-10 Display for ΔH=35 gamma

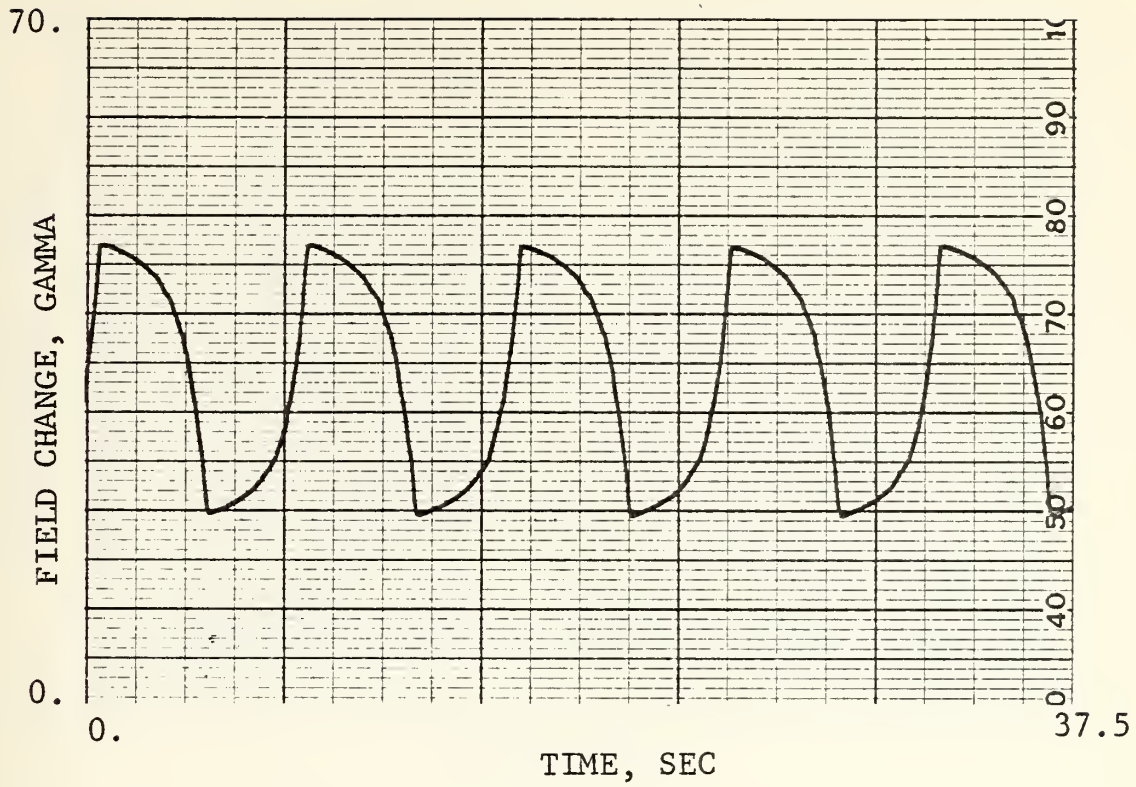

Figure 5.13 Pen Recorder Output for ΔH= 28 gamma

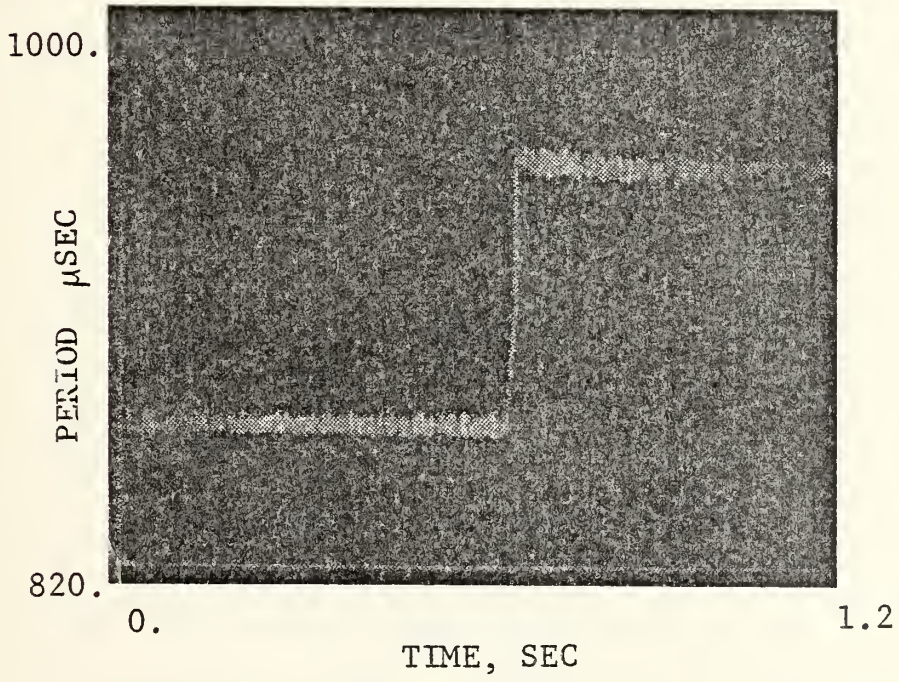

Figure 5.14 AGT-10 Display for ΔH= 28 gamma

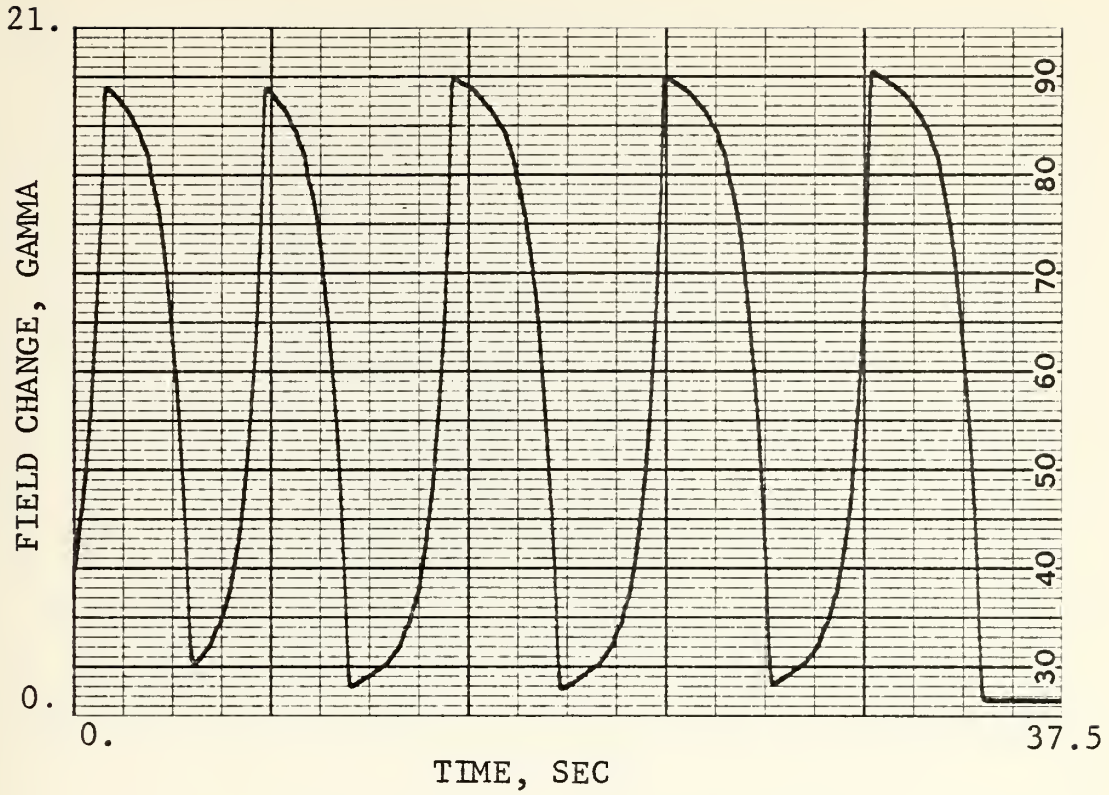

Figure 5.15 Pen Recorder Output for ΔH= 18 gamma

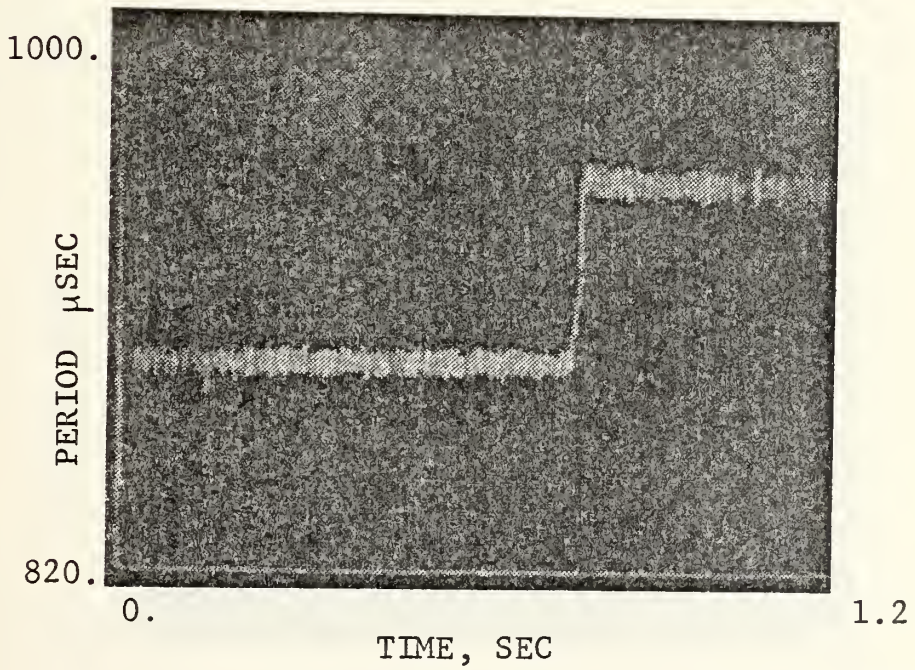

Figure 5.16 AGT-10 Display for ΔH= 18 gamma

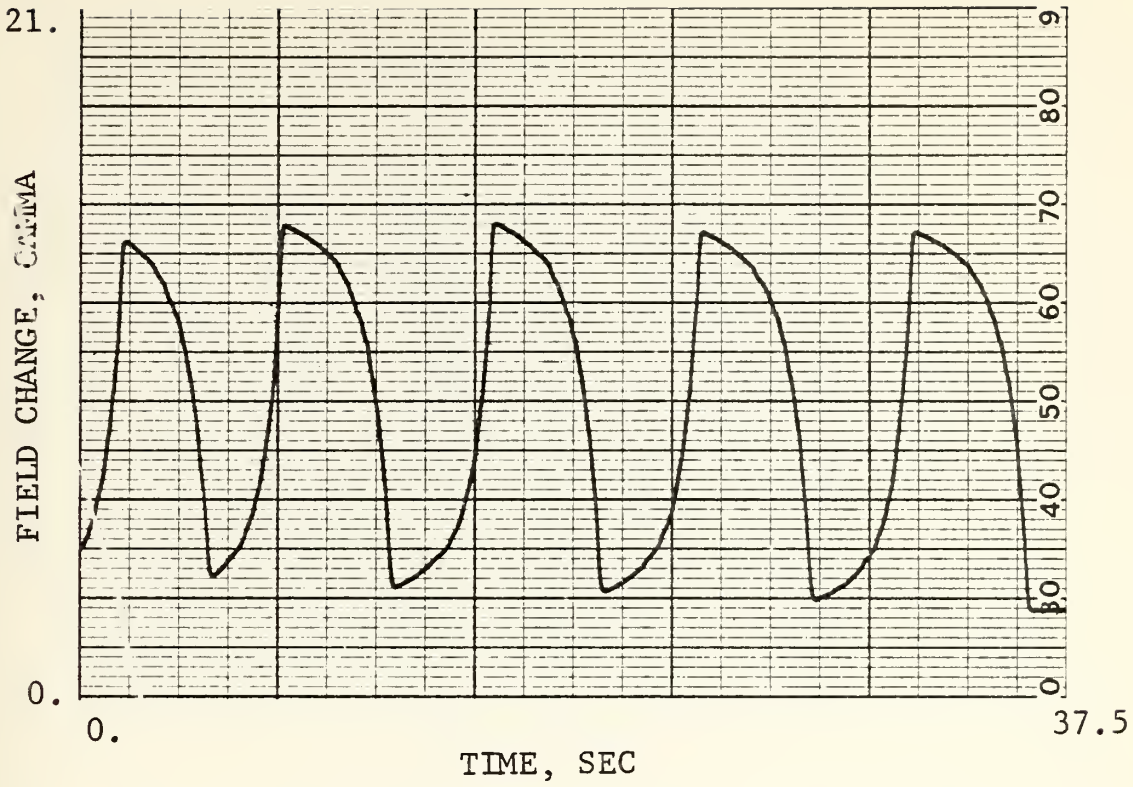

Figure 5.17 Pen Recorder Output for ΔH= 11 gamma

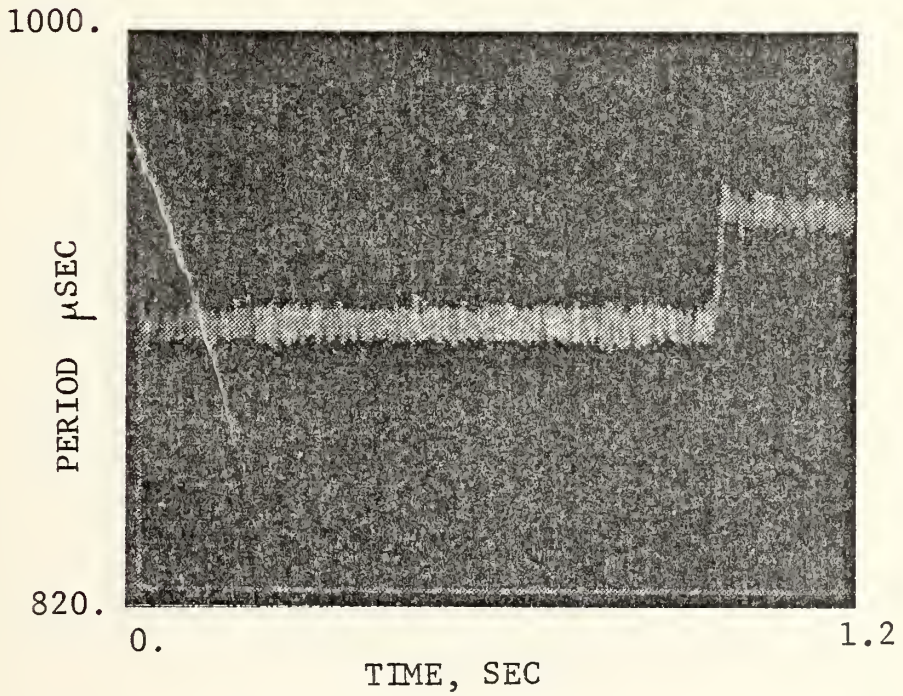

Figure 5.18 AGT-10 Display for ΔH= 11 gamma

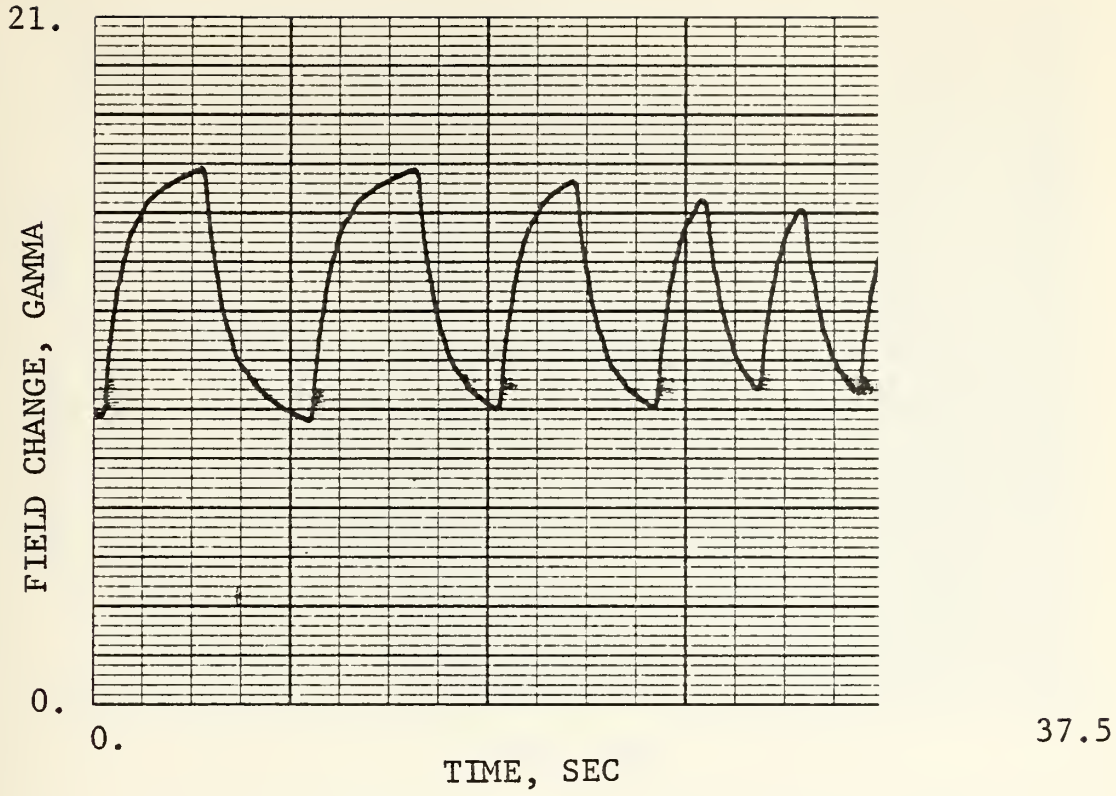

Figure 5.19 Pen Recorder Output for $\Delta H = 8$ gamma

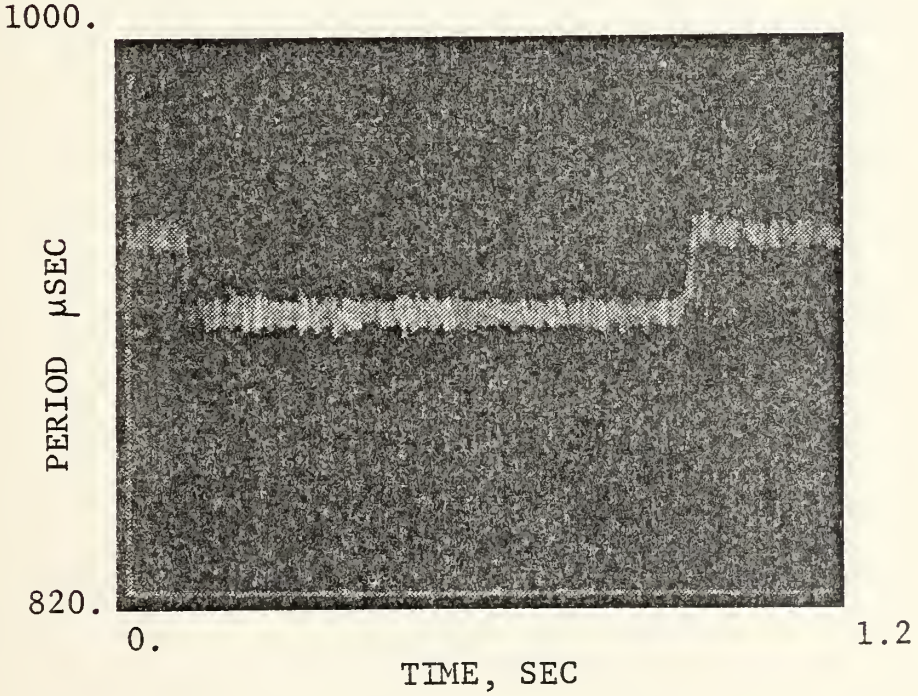

Figure 5.20 AGT-10 Display for $\Delta H = 8$ gamma

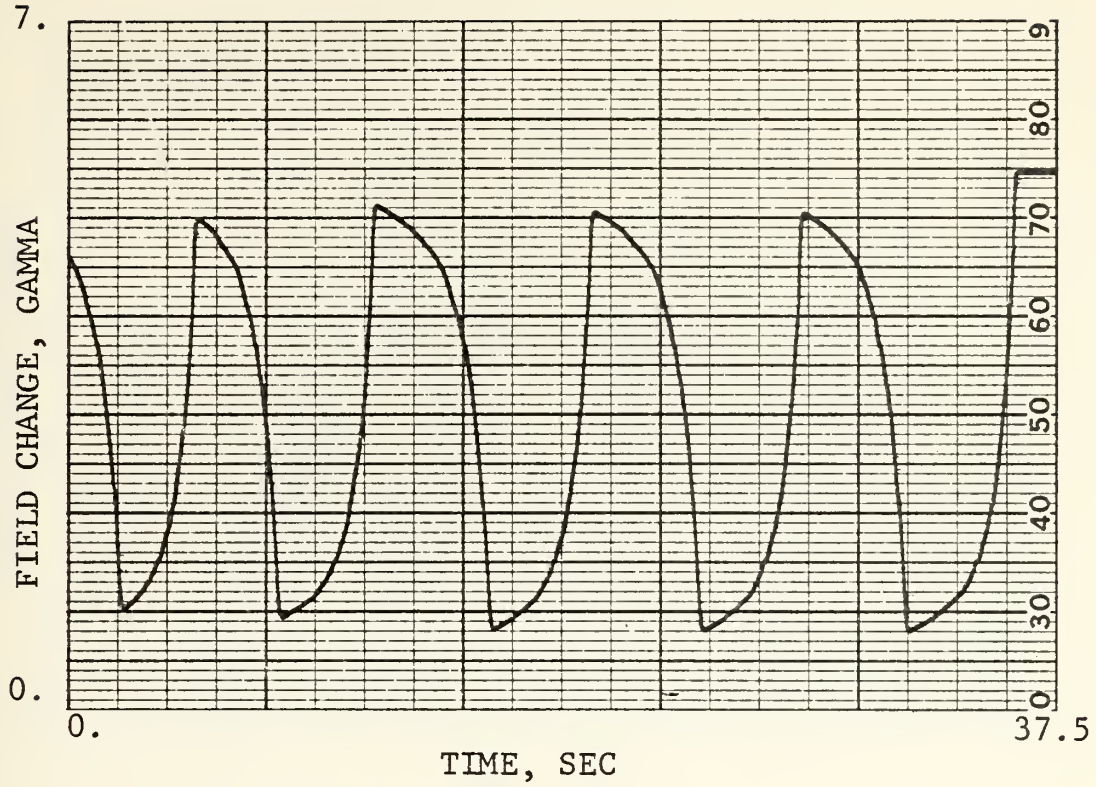

Figure 5.21 Pen Recorder Output for $\Delta H = 4$ gamma

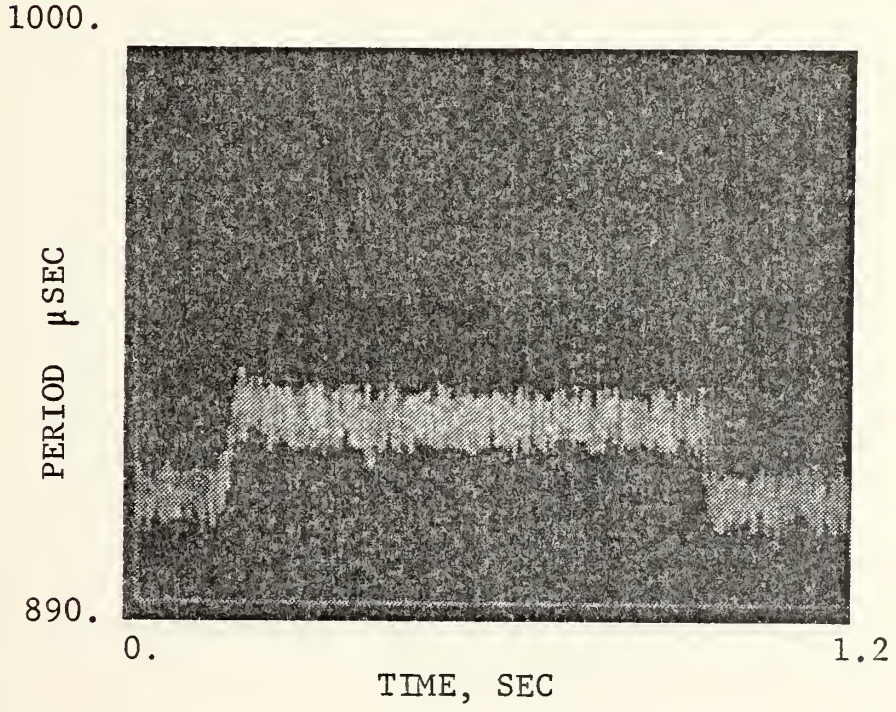

Figure 5.22 AGT-10 Display for $\Delta H = 4$ gamma

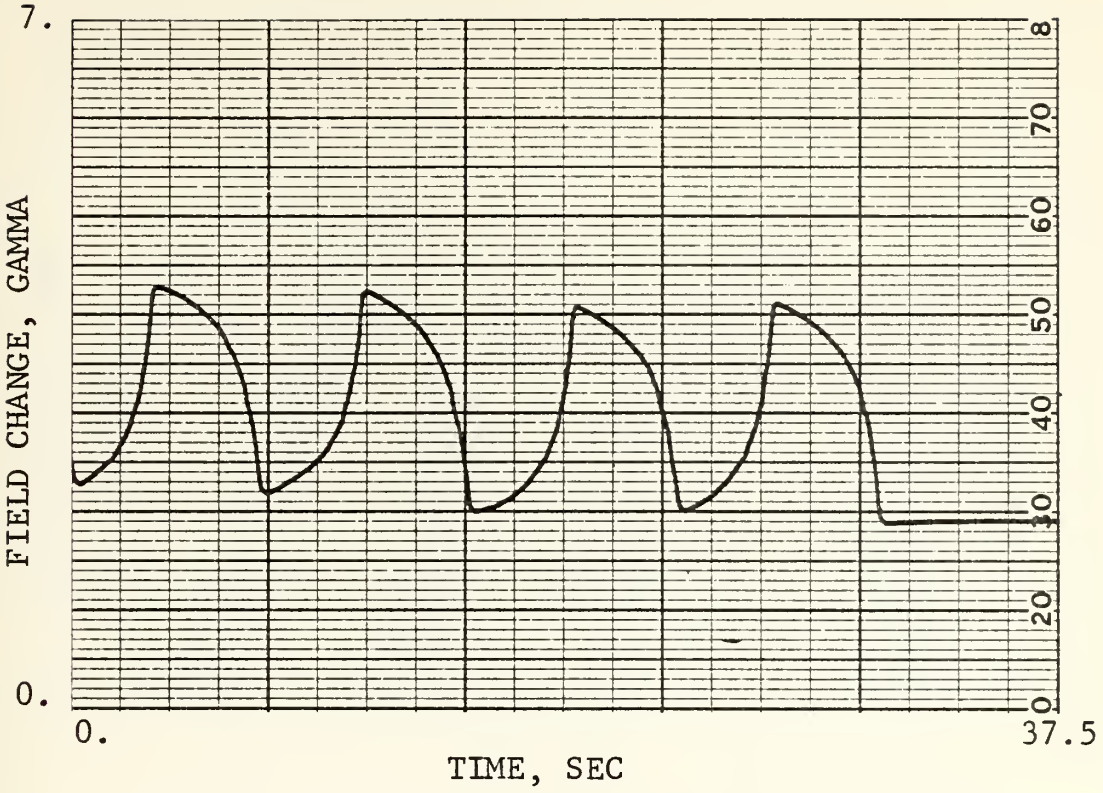

Figure 5.23 Pen Recorder Output for $\Delta H = 2$ gamma

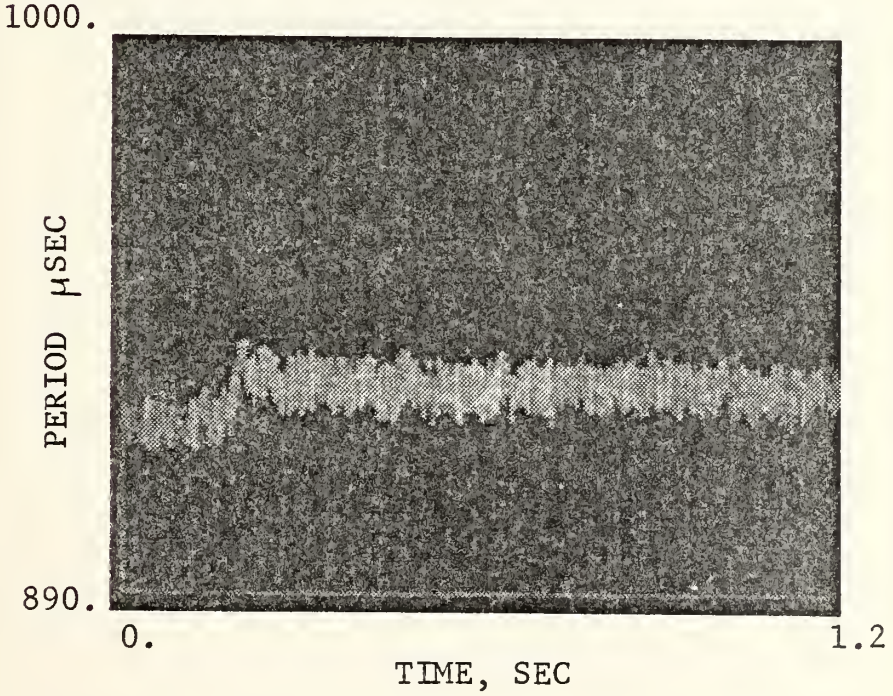

Figure 5.24 AGT-10 Display for $\Delta H = 2$ gamma

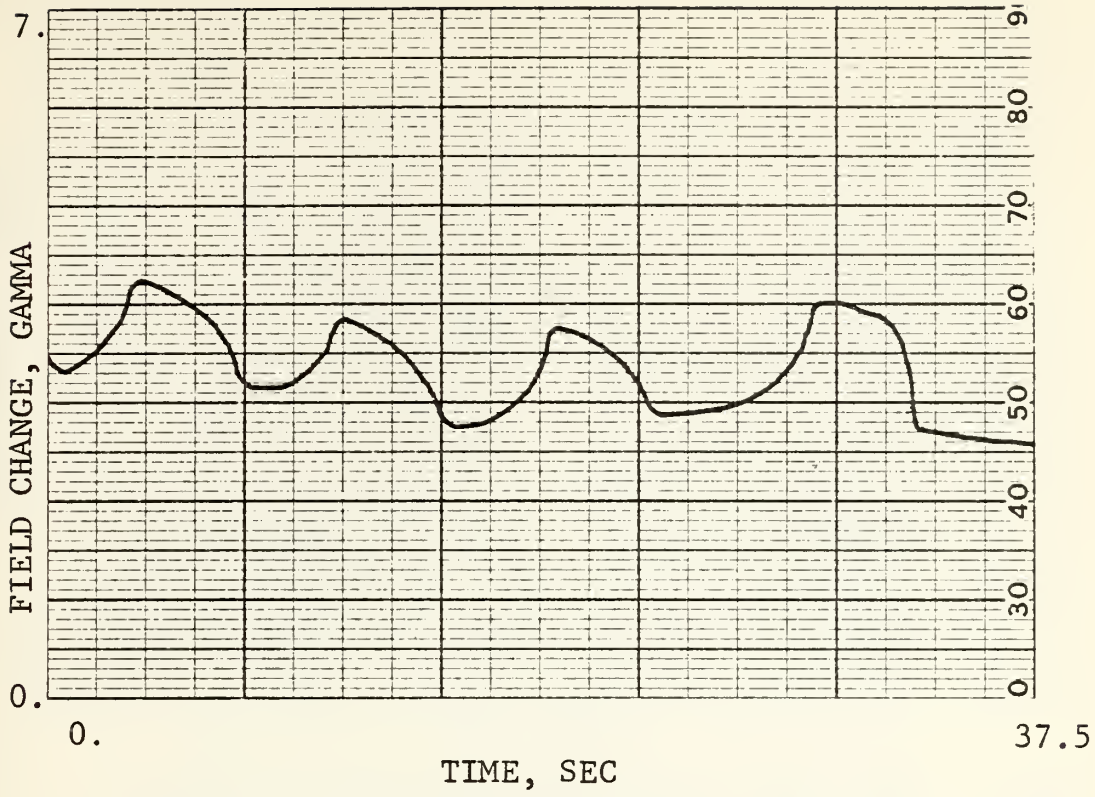

Figure 5.25 Pen Recorder Output for $\Delta H = 1$ gamma

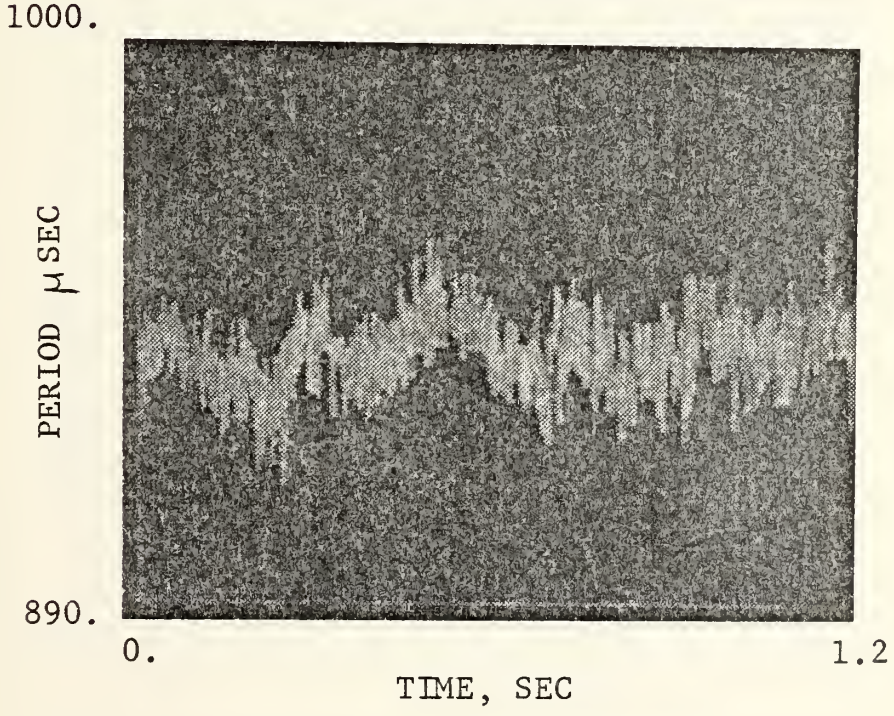

Figure 5.26 AGT Display for $\Delta H = 1$ gamma

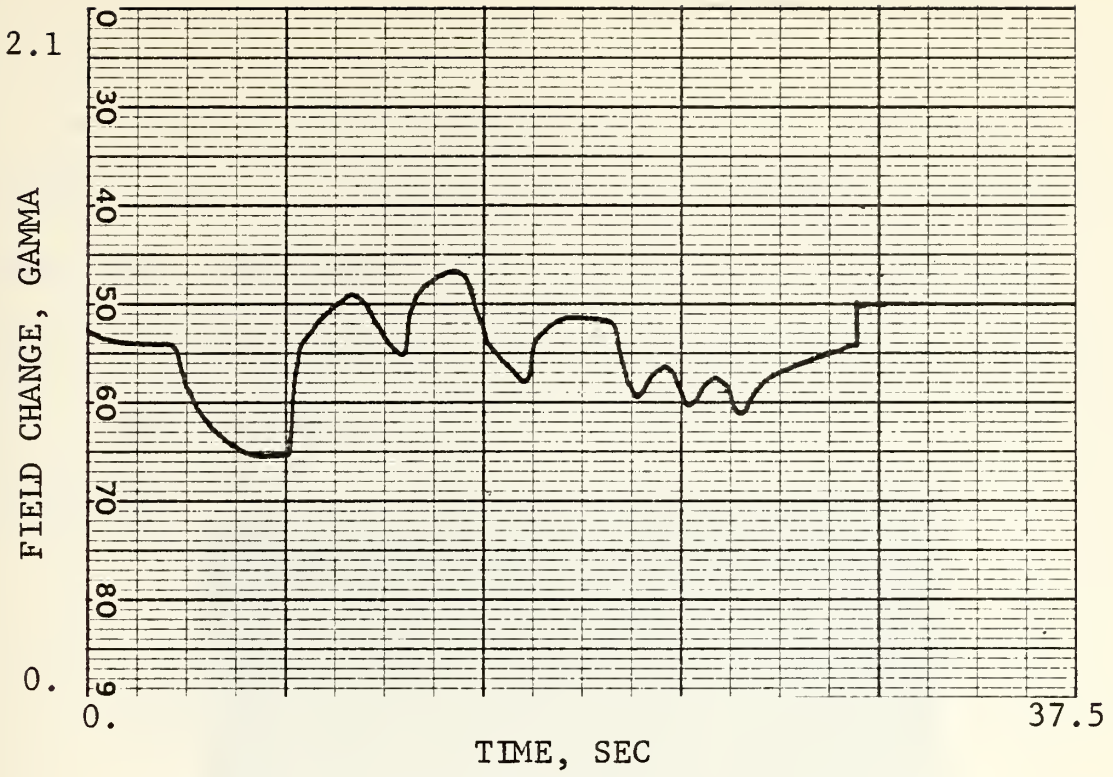

Figure 5.27 Pen Recorder Output for $\Delta H = .6$ gamma

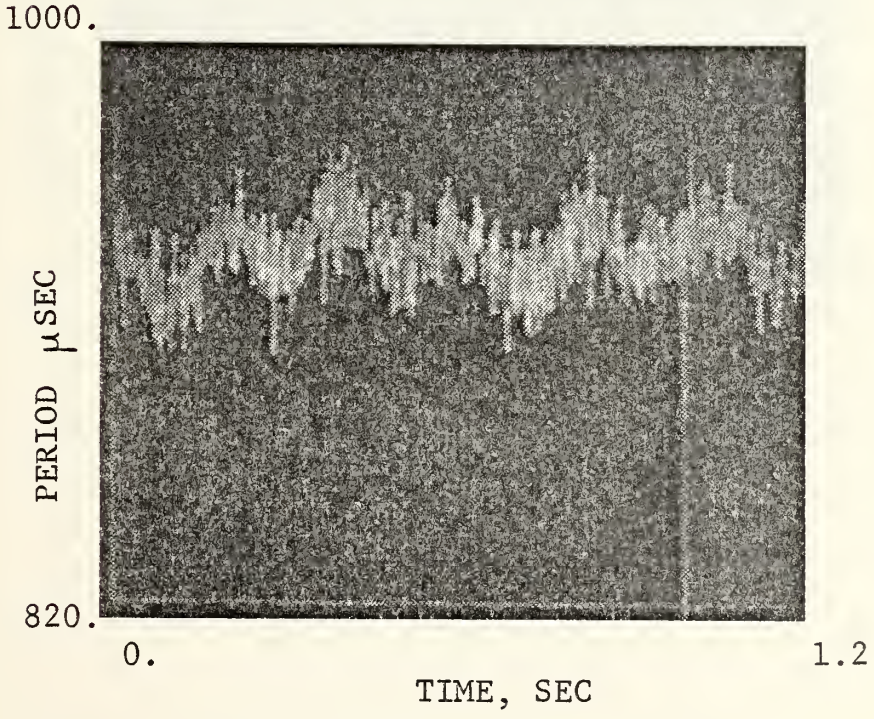

Figure 5.28 AGT-10 Display for $\Delta H = .6$ gamma

To obtain a precise measurement of the magnetometer's response time the AGT-10 display was expanded. Figure 5.29 shows the rising edge and Figure 5.30 the falling edge. As seen the rising edge required approximately three periods or 2.5 msec to respond and the falling edge only one period or .8 msec.

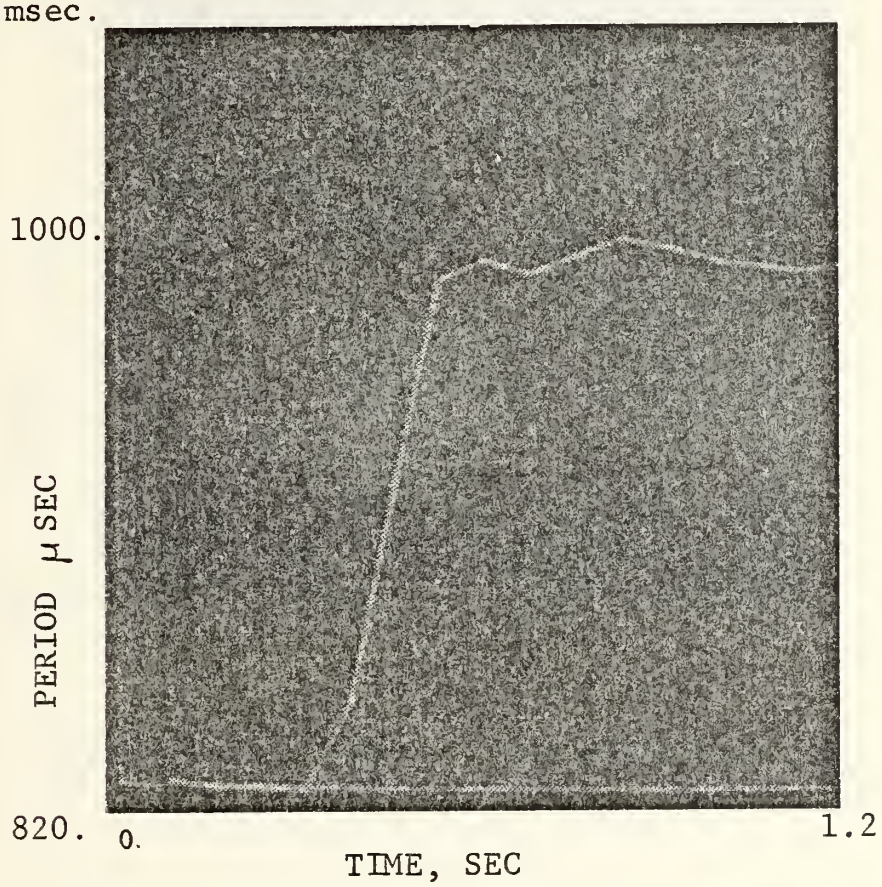

Figure 5.29 Expanded View of Rising Edge of Magnetometer Response

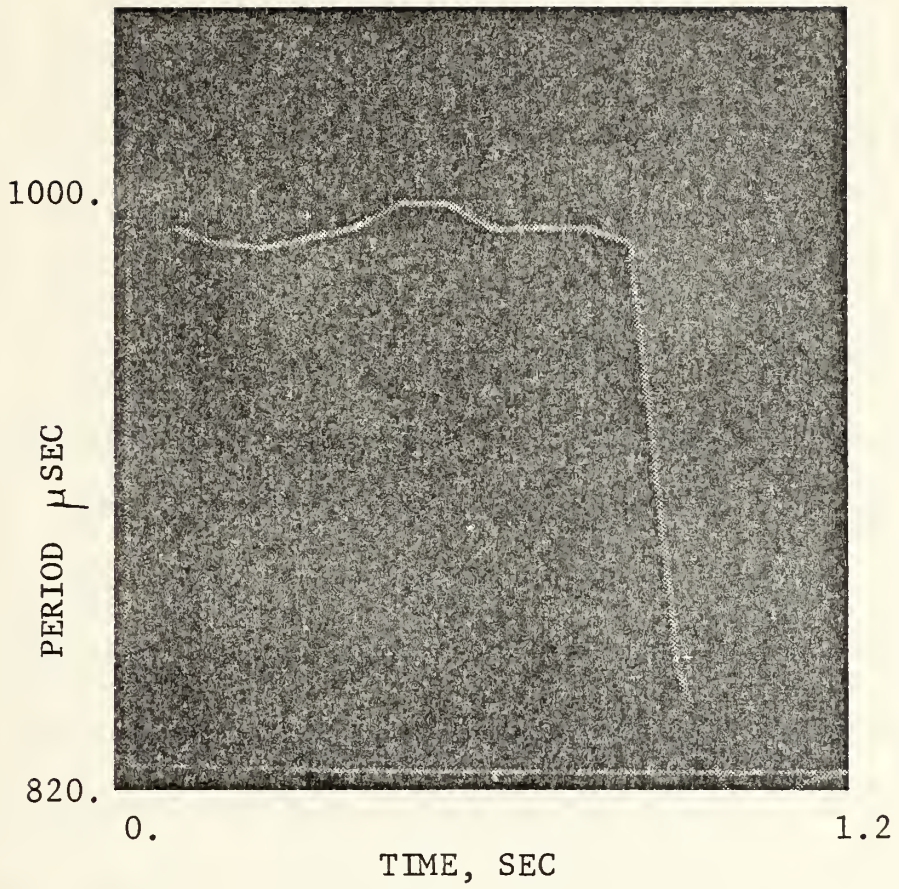

Figure 5.30 Expanded View of Falling Edge of Magnetometer Response

The periodmeter and interface unit measured the period of the signal with an absolute accuracy of .75 μsec and properly input the value to the computer. The resolution of the device was .25 μsec using a 4 MHz time base and this could be increased by using a faster time base. The system was successfully operated with a 10 MHz clock frequency and resolution of .1 μsec. The use of an increased clock frequency or averaging of periods to increase the periodmeters resolution would not improve the system sensitivity. The overall system sensitivity is limited by the flutter and noise of the tape recorder. Two methods were attempted to overcome this: 1) the use of a synchronized oscillator constructed of two multivibrators synchronized with the zero crossings of the input signal; 2) recording a 1 kHz reference signal on a second channel of the recorder and multiplying it up for use as a time base. The pulse width instability of the multivibrators was greater than the flutter noise so the synchronized oscillator was unsatisfactory. A phase lock loop type frequency multiplier was constructed to multiply the 1 kHz to 1 MHz but the delay time through the loop was too great to cancel the flutter for a period to period measurement.

To achieve greater system sensitivity and resolution some means of flutter cancellation is necessary.

APPENDIX A

OPTICAL PUMPING OF THE CESIUM ATOM

Figure A-1 shows the energy levels of the cesium atom. Absorption of photons of light by the cesium valence electrons cause their energy to be increased from the $^2S_{\frac{1}{2}}$ ground state to the $^2P_{\frac{1}{2}}$ state. Due to the light's polarization the magnitude of the quantum number m is also increased by one. An excited atom quickly emits its energy and returns to any of the ground state sublevels. The absorption and re-emission is repeated resulting in a shift to the m=+4 sublevel. Since the $^2P_{\frac{1}{2}}$ state contains no m level above +4, transitions out of the $^2S_{\frac{1}{2}}$, m=+4 level are not possible. This is precisely optical pumping and under these conditions there can be no further absorption of light.

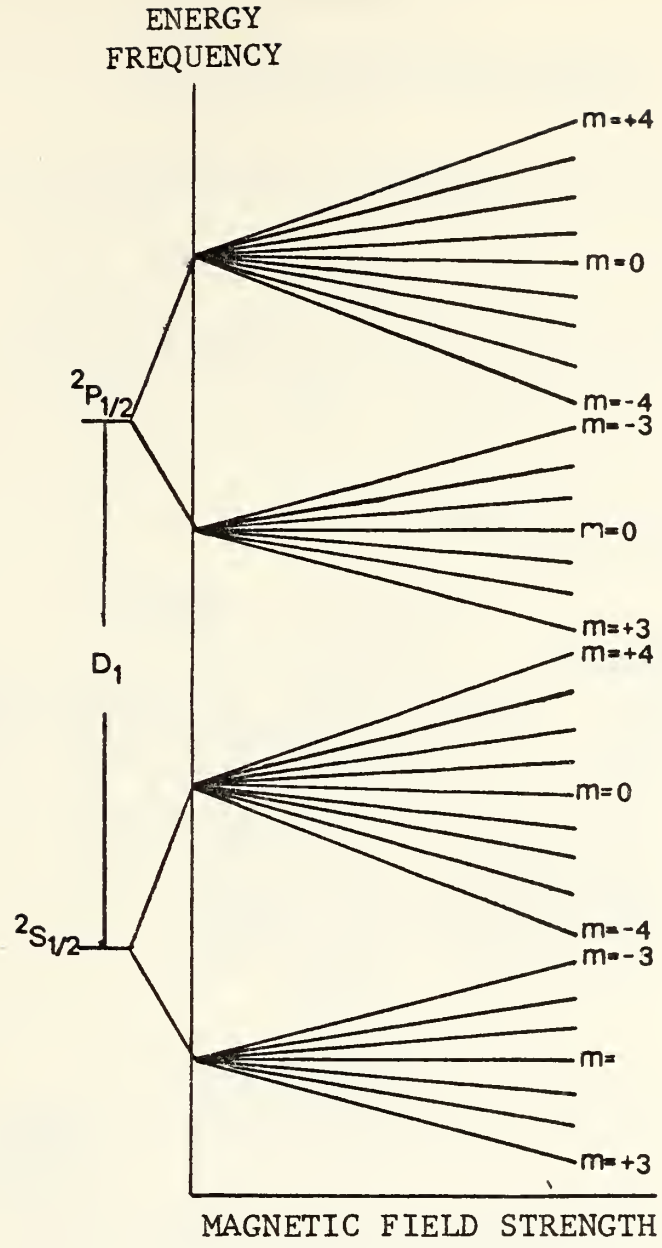

Figure A-1 Energy Levels of Cesium Atom

APPENDIX B

OPTICAL DETECTION SYSTEMS

The first method used to obtain a continuous record of the total field intensity used a control loop arrangement and was therefore called a Controlled Magnetometer. A block diagram of it is shown in Figure B-1.

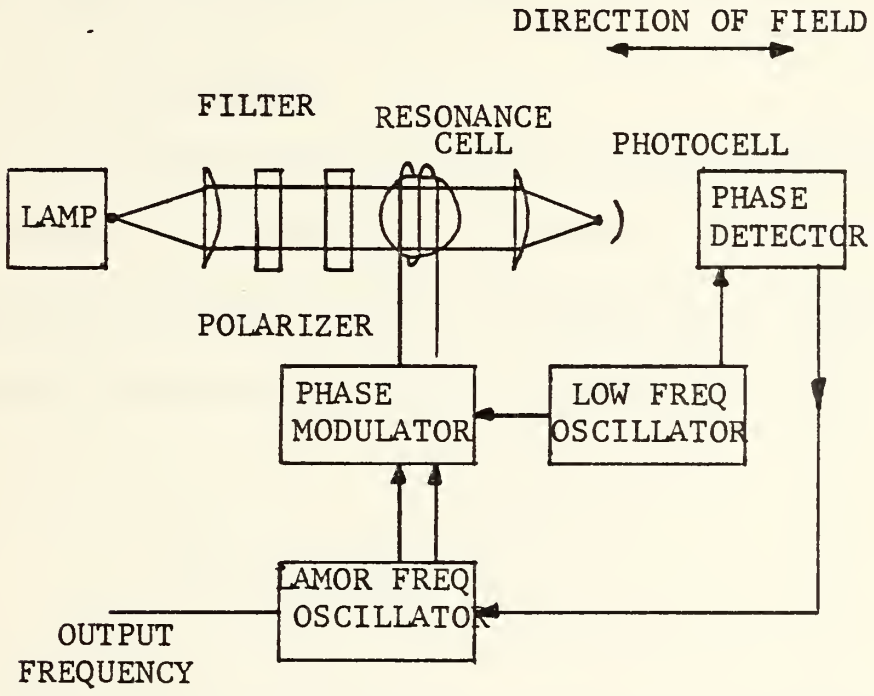

Figure B-1 Controlled Magnetometer

A small frequency modulation is applied to the local RF oscillator to sweep it back and forth through resonance. Owing to this sweeping the signal collected at the photocell is also modulated at the same frequency, but its phase

with respect to the initial modulating signal depends on the position of the local RF with respect to the resonant frequency. The photocell output and modulating signal are phase detected and the output is used as an error signal in a control loop to maintain the local RF oscillator coincicent with the resonant frequency. This system does not place severe restrictions on the performance of the photocell or its amplifier, has high accuracy, good stability, and good low field capability.

One attribute the controlled system does not have is a good response to transients. Figure B-2 shows the block diagram of a system that has the excellent response to transients necessary to detect and observe micropulsations.

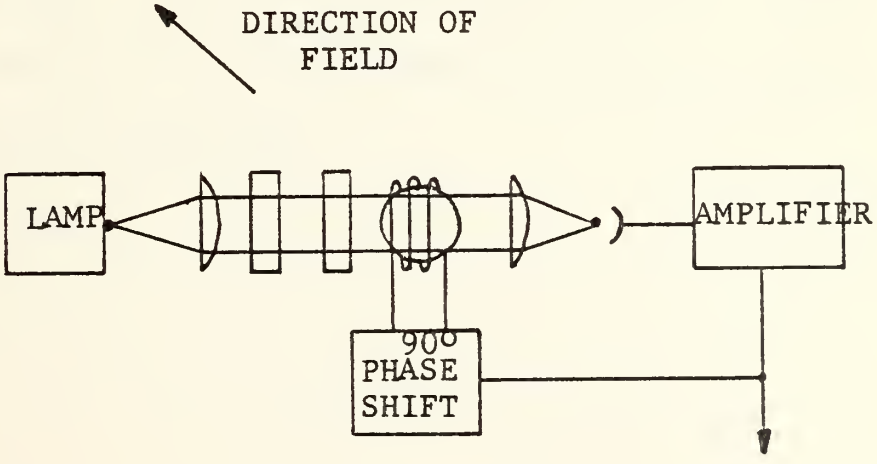

Figure B-2 Self-Oscillating Magnetometer

In theory a second light beam is placed at right angle with respect to the first and the variation of the M_x component of the magnetization is observed. Since this transverse component oscillates at the frequency of the signal injected and the amplitude is a maximum at resonance, the photocell is simply amplified, phase shifted, and re-injected to the coils. The system will then oscillate at the resonant frequency. In practice it is possible to use a single light beam inclined at 45^{o} to the direction of the field to be measured. This places an orientation restriction on the sensor, but systems employing two and three resonance cells have been developed that overcome this. This system places severe restrictions on the amplifier and especially on the accuracy of the phase shift, which is required to maintain oscillation. It has a low absolute accuracy and poor long term stability but as previously mentioned, excellent response to transients.

APPENDIX C

PERIODMETER AND INTERFACE CIRCUITS

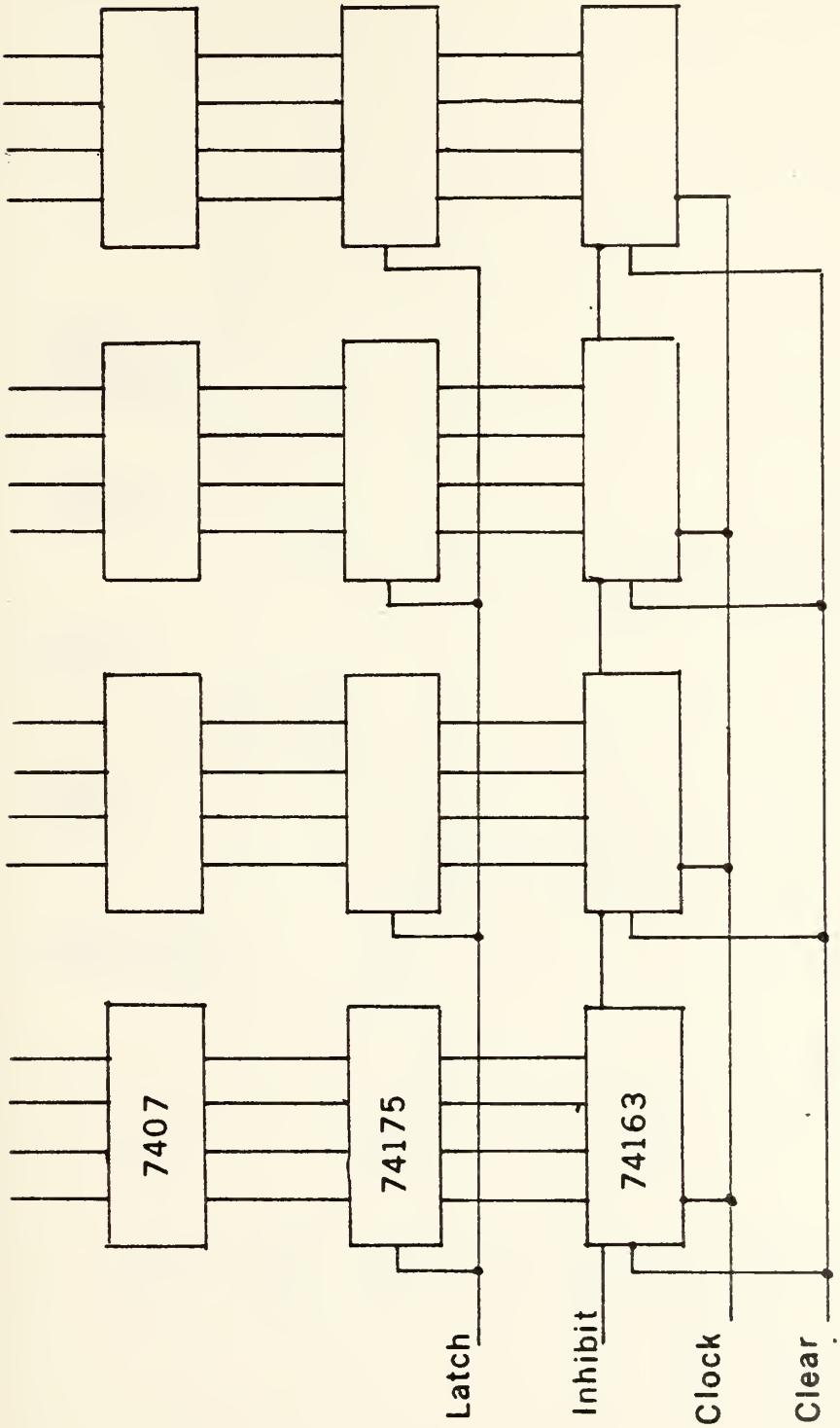

Figure C-1 Counting Circuitry

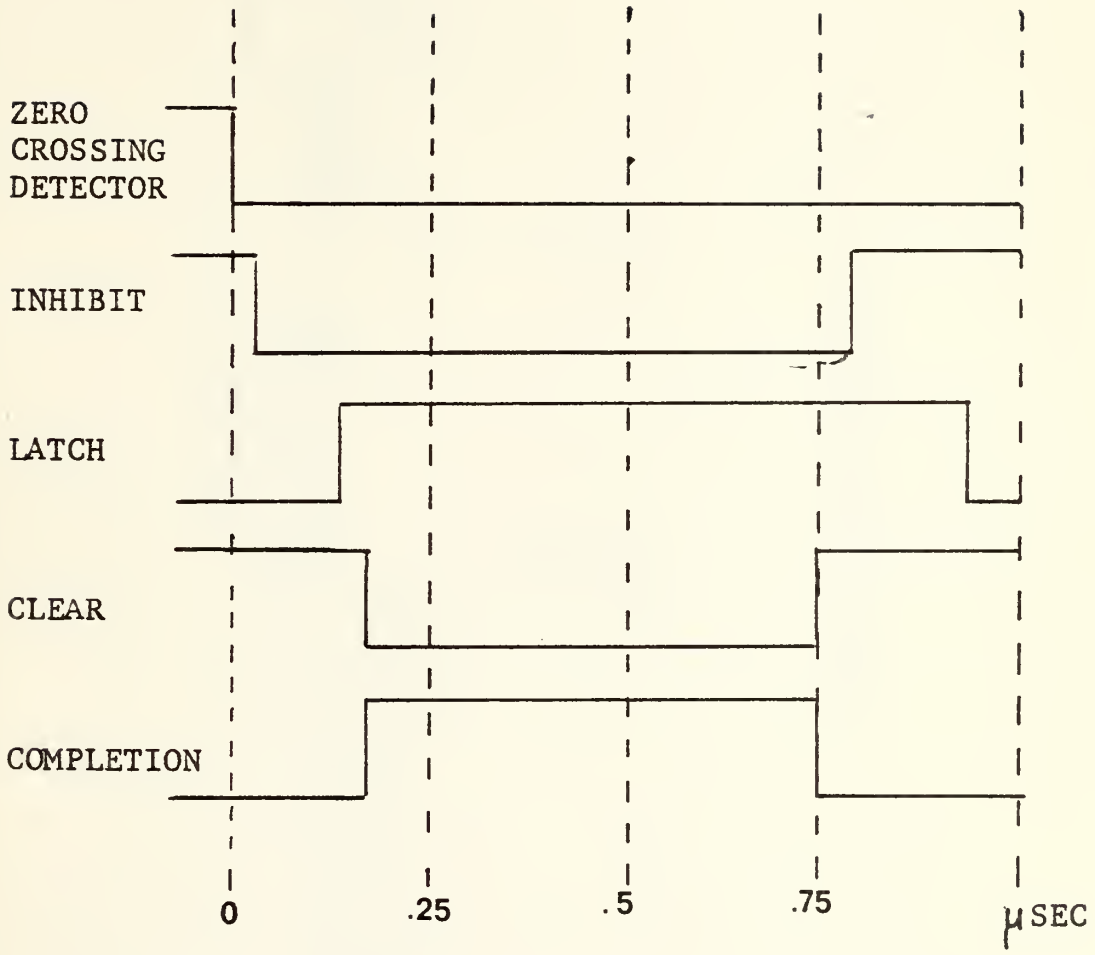

Figure C-2 Input Circuitry Timing Diagram

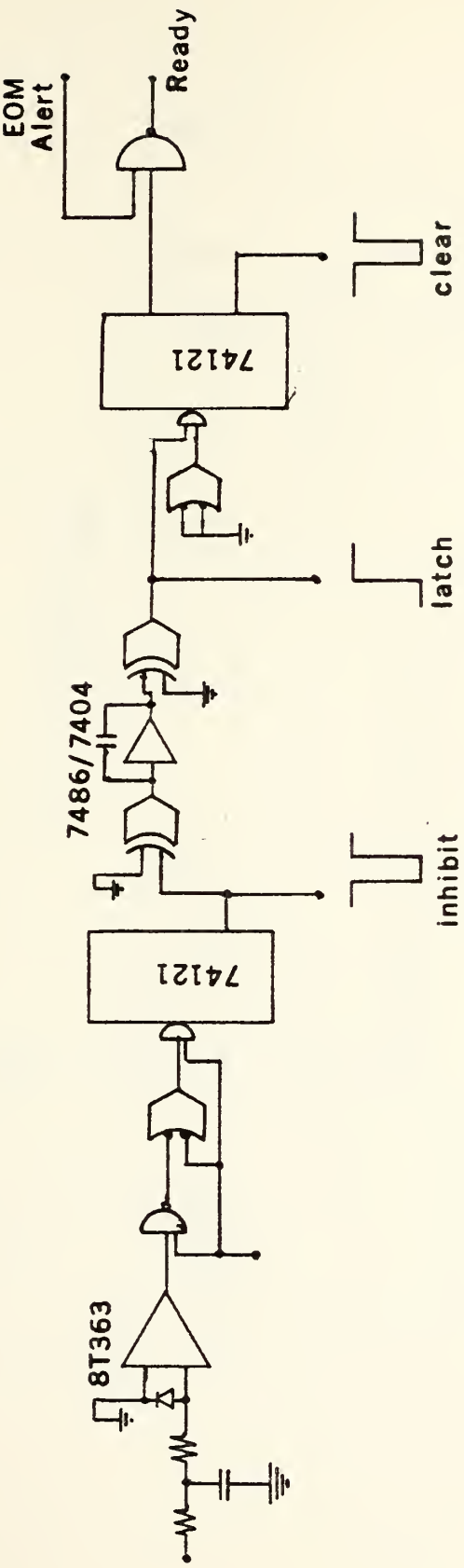

Figure C3 Input Circuitry

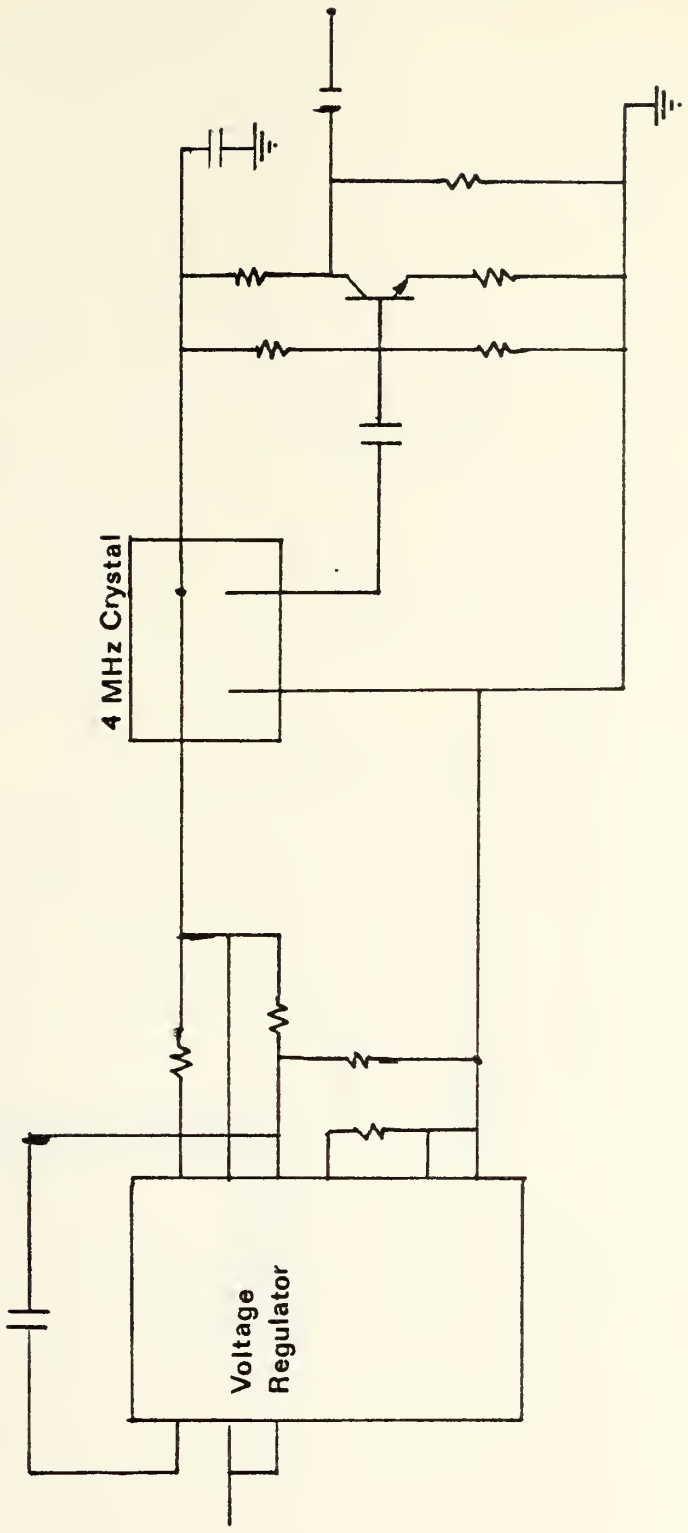

FIGURE C4 TIME BASE

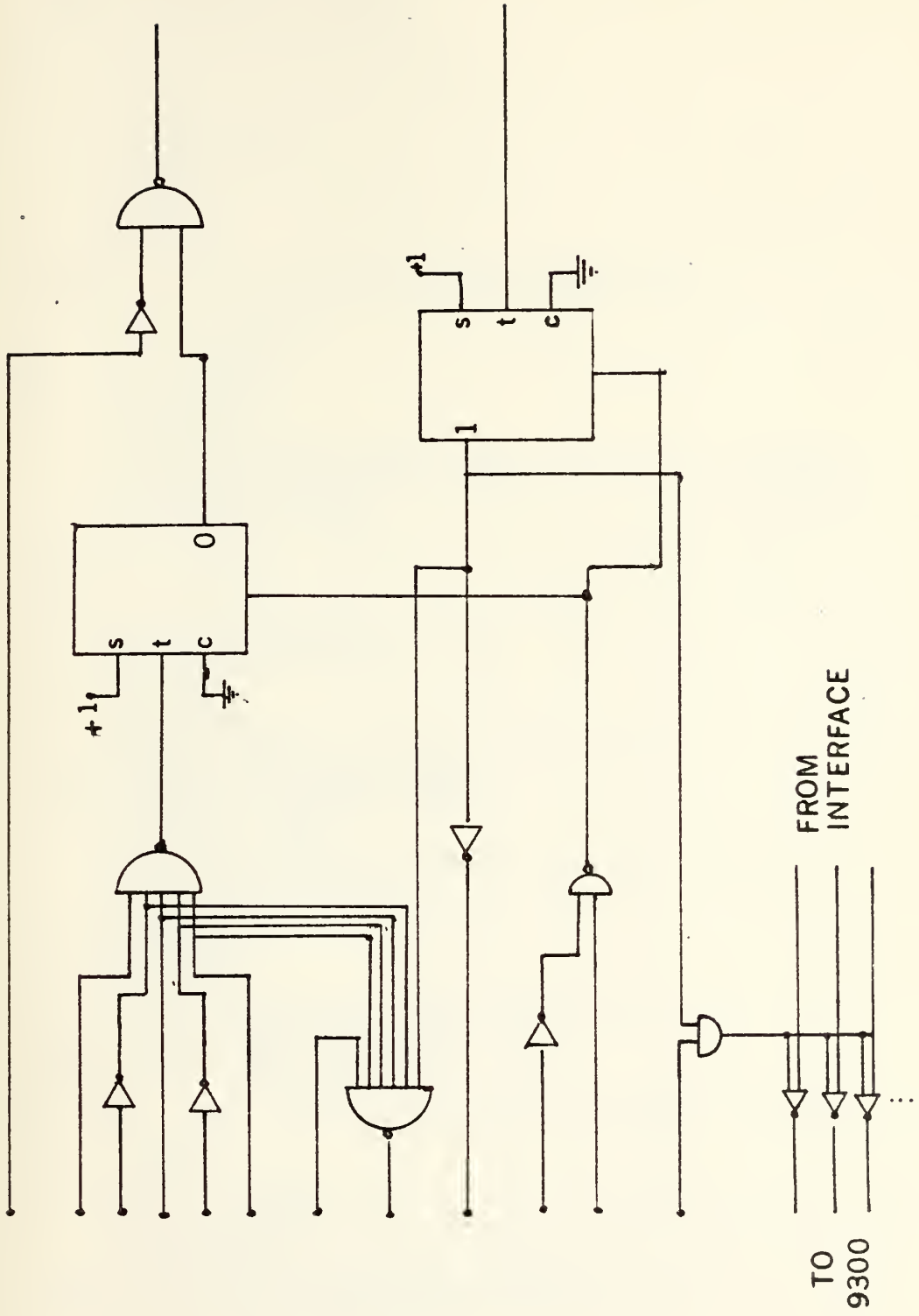

FIGURE C·5 COMPUTER INTERFACE

```
-JOB
-FORTRAN LS,GO,S
      DIMENSION COUNT(13000),IVAR(6)
      INTEGER COUNT
      DATA NSAMP,MULT/4096,3/
      LBLK=NSAMP*MULT
  106 FORMAT(1X,12(I10))
  999 CONTINUE
C
CC    INITIALIZE VARIALBLES
C
      IMAX=1
      IMIN=100000
      SUM=0.
      SUMSQ=0.
      C=0.
      IBAD=0
      BAD=0.
C
CC   INPUT DATA FROM PERIPHERAL/INTERFACE
C
      DO 2 I=1,LBLK
SSS   ECM 032400
SSS   SKS 032400
SSS   EBL $-1
S     PIN ITEM
      ICOUNT =0
      ICOUNT=LAND(ITEM,177B)
      ICOUNT=LIOR(ICOUNT,LAND(LRS(ITEM,1),376000B))
      ICOUNT=LIOR(ICOUNT,LAND(LRS(ITEM,1),1400000B))
      COUNT(I)=ICOUNT
    2 CONTINUE
C
CC  FORM AN INITIAL AND THEN PRECISE MEAN & SDEV
C
      DO 3 I=1,LBLK
      SUM=SUM+COUNT(I)
      SUMSQ=SUMSQ+COUNT(I)**2
      C=C+1.0
    3 CONTINUE
      MEAN=SUM/C
      SDEV=SQRT(ABS(C*SUMSQ-SUM**2))/C
      WRITE(6,100)MEAN,SDEV
  100 FORMAT('0 MEAN=',F12.4/
     1' SDEV=',F12.4)
      DO 4 I=1,LBLK
      IF(ABS(COUNT(I)-MEAN).LE.5.*SDEV) GO TO 4
      SUM=SUM-COUNT(I)
      SUMSQ=SUMSQ-COUNT(I)**2
      BAD=BAD+1.
    4 CONTINUE
      C=C-BAD
      MEAN=SUM/C
      SDEV=SQRT(ABS(C*SUMSQ-SUM**2))/C
      WRITE(6,101)MEAN,SDEV
  101 FORMAT('0 TRUE MEAN=',F12.4/
     1' TRUE SDEV=',F12.4)
C
CC    FORM A NEW ARRAY CONSISTING OF POINTS WITHIN 10 SDEV
C
      IBAD=0
      NEWI=0
      DO 6 I=1,LBLK
      IF(ABS(COUNT(I)-MEAN).LE.10.*SDEV)NEW=NEWI+1;GO TO 7
      IBAD=IBAD+1
      WRITE(6,102) IBAD,I,COUNT(I)
  102 FORMAT('0 THIS IS BAD POINT NO',I5/
     1' ITS OLD SUBSCRIPT WAS',I8/
     2' ITS VALUE WAS',I10)
      GO TO 6
    7 COUNT(NEWI)=COUNT(I)
    6 CONTINUE
```

```
      DO 15 I=NEWI+1,LBLK
      COUNT(I)=0
   15 CONTINUE
      WRITE(6,103) NEWI
  103 FORMAT('0 NEWI=',I10)
C
CC ZERO FILL ARRAY FROM LAST POINT TO END OF BLOCK
C
      DO 8 I=NEWI+1,LBLK
      COUNT(I)=0
    8 CONTINUE
C
CC  FIND A MINIMUM AND MAXIMUM VALUE
C
      DO 9 I=1,NEWI
      IMIN=AMIN0(COUNT(I),IMIN)
      IMAX=AMAX0(COUNT(I),IMAX)
    9 CONTINUE
      WRITE(6,104)IMIN,IMAX
  104 FORMAT('0 MINIMUM=',I10/
     1' MAXIMUM=',I10)
C
CC  BUFFEROUT TO TAPE THE ARRAY IVAR CONTAINING VARIABLES
C
      IVAR(1)=NEWI
      IVAR(2)=MEAN
      IVAR(3)=SDEV
      IVAR(4)=IMIN
      IVAR(5)=IMAX
      WRITE(6,105)(IVAR(I),I=1,5)
  105 FORMAT(1X,5I10)
      OUTPUT(102)'WRITE ON TAPE'
      READ(101,601)IANSS
  601 FORMAT(A4)
      IF(IANSS.NE.3HYES) GO TO 603
      CALL BUFFEROUT(1,1,IVAR,5,IND)
   11 IF(IND.EQ.1) GO TO 11
C
CC  BUFFEROUT TO TAPE THE ARRAY COUNT IN GROUPS OF 4096
C
      DO 12 I=1,MULT
      J=I-1
      K=(J*NSAMP)+1
      CALL BUFFEROUT(1,1,COUNT(K),NSAMP,IND)
   13 IF(IND.EQ.1) GO TO 13
   12 CONTINUE
  603 CONTINUE
      OUTPUT(102) 'READ ANOTHER 14336'
      READ(101,600)IANS
  600 FORMAT(A4)
      IF(IANS.EQ.3HYES) GO TO 999
      END
-LOAD XR,MAP
-DATA
```

```
$PATCH
$>>DATA
007067  00106711
$END
-AGT
-JCE
-FORTRAN LS,GO
      DIMENSION IAXIS(10),INDATA(4105),DATA(4105),IVAR(6),
     1IGDIR(5),ITDIR(15),ITEXT(24),T(3)
      INTEGER RESP(4)
      DATA NSAMP,MULT,NDIS/4096,3,16/
      IDEV=1
      LBLK=NSAMP*MULT
      DIV=FLOAT(NDIS)
      NBLK=1
      IAXIS(1)=IHEAD(0,10)
      IAXIS(2)=IPACK(-.5,.75,0)
      IAXIS(3)=IPACK(-.5,1.,0)
      IAXIS(4)=IPACK(-.5,0.,1)
      IAXIS(5)=IPACK(0.,0.,1)
      IAXIS(6)=IPACK(0.,-.01,1)
      IAXIS(7)=IPACK(0.,0.,0)
      IAXIS(8)=IPACK(.5,0.,1)
      IAXIS(9)=IPACK(.5,-.01,1)
  999 CONTINUE
      TIME=0.
      LREC=NSAMP
    2 CALL FNS(IDEV,ISW,IER)
      IF(IER.NE.0) OUTPUT(101)IER,'F1'
      IF(ISW.NE.0) GO TO 2
C
CC BUFFERIN ARRAY IVAR WITH VARIABLES
C
      CALL BUFFERIN(1,1,IVAR,5,INC)
    3 IF(INC.EQ.1) GO TO 3
      NEW1=IVAR(1)
      MEAN=FLOAT(IVAR(2))/4.
      SDEV=FLOAT(IVAR(3))/4.
      MIN=FLOAT(IVAR(4))/4.
      MAX=FLOAT(IVAR(5))/4.
      WRITE(6,800)(IVAR(I),I=1,5)
  800 FORMAT(1X,'NO. OF POINTS=',I10/
     1' MEAN=',I10/
     2' SDEV=',I10/
     3' MINIMUM=',I10/
     4' MAXIMUM=',I10)
C
CC   WRITE MEAN,SDEV,MIN,MAX ON SCREEN
C
      CALL DGINIT(IDEV,IGDIR,5,IER)
      IF(IER.NE.0)OUTPUT(101)IER,'DG1'
      CALL DTINIT(IDEV,ITDIR,15,IER)
      IF(IER.NE.0) OUTPUT(101) IER,'D2'
      ENCODE(96,200,ITEXT)
  200 FORMAT('PERIOD')
      CALL TEXTO(IDEV,ITEXT,24,3,26,1,3,IER)
      IF(IER.NE.0)OUTPUT(101)IER,'PERIOD'
      ENCODE(96,201,ITEXT)
  201 FORMAT('T SEC')
      CALL TEXTO(IDEV,ITEXT,24,22,75,1,3,IER)
      IF(IER.NE.0)OUTPUT(101)IER,'PTIME'
      ENCODE(96,303,ITEXT)NBLK
  303 FORMAT('STATISTICS ON BLOCK',I3)
      CALL TEXTO(IDEV,ITEXT,24,24,32,1,3,IER)
      IF(IER.NE.0) OUTPUT(101)IER,'TE1'
      ENCODE(96,304,ITEXT)MEAN,SDEV
  304 FORMAT('MEAN VALUE=',F8.3,4X,'SDEV=',F8.3)
      CALL TEXTO(IDEV,ITEXT,24,25,24,1,3,IER)
      IF(IER.NE.0) OUTPUT(101)IER,'TE2'
      ENCODE(96,306,ITEXT) MIN,MAX
  306 FORMAT('MIN PERIOD IN MICROSEC=',F8.3,
     14X,'MAX PERIOD=',F8.3)
```

```
      CALL TEXTO(IDEV,ITEXT,24,26,24,1,3,IER)
      IF(IER.NE.0) OUTPUT(101)IER,'TE3'
      ENCODE(96,308,ITEXT)
  308 FORMAT('SET MIN & MAX VALUE OF Y AXIS IN MICRSEC')
      CALL TEXTO(IDEV,ITEXT,24,28,24,1,3,IER)
      IF(IER.NE.0) OUTPUT(101)IER,'TE4'
      ENCODE(96,310,ITEXT)
  310 FORMAT('TYPE A MIN,A COMMA, AND MAX IN AN F FORMAT')
      CALL TEXTO(IDEV,ITEXT,24,29,24,1,3,IER)
      IF(IER.NE.0)OUTPUT(101)IER,'PTYPE'
      ENCODE(96,309,ITEXT)
  309 FORMAT('TO USE STATISTICAL MIN AND MAX AS Y AXIS
     1MIN AND MAX TYPE JUST A C/R')
      CALL TEXTO(IDEV,ITEXT,24,32,24,1,3,IER)
      IF(IER.NE.0) OUTPUT(101) IER,'T1'
   42 CALL TEXTR(IDEV,77777778,1,30,24,1,3,IER)
      IF(IER.NE.0)OUTPUT(101)IER,'TXTR'
   40 IF(MOD(ITDIR(9),8).EQ.0) GO TO 40
      CALL TEXTI(IDEV,RESP,4,0,9,IER)
      IF(RESP(1).NE.0H) GO TO 41
      DMIN=MIN
      DMAX=MAX
   41 CONTINUE
      DECODE(16,120,RESP)DMIN,DMAX
  120 FORMAT(2F8.0)
      IF(DMIN.GE.DMAX) GO TO 42
      DMAX2=DMAX-DMIN
      ENCODE(96,315,ITEXT)DMIN
  315 FORMAT(F8.2)
      CALL TEXTO(IDEV,ITEXT,24,20,20,1,3,IER)
      IF(IER.NE.0)OUTPUT(101)IER,'LAST'
      ENCODE(96,316,ITEXT)DMAX
  316 FORMAT(F8.2)
      CALL TEXTO(IDEV,ITEXT,24,5,20,1,3,IER)
      IF(IER.NE.0)OUTPUT(101)IER,'LAST+1'
      KKK=1
  998 CONTINUE
C
CC    BUFFERIN 4096 POINTS OF ARRAY COUNT INTO INDATA
C
      IDEV=1
      CALL BUFFERIN(1,1,INDATA,NSAMP,INC)
    4 IF(INC.EQ.1) GO TO 4
      IF((NBLK.LE.11).OR.(NBLK.GE.14)) GO TO 801
      DO 27 L1=1,4081,16
      WRITE(6,106)(INDATA(L2),L2=L1,L1+15)
  106 FORMAT(1X,16(I6,2X))
   27 CONTINUE
  801 CONTINUE
C
CC    MAKE INDATA A REAL ARRAY
C
      DO 10 I=1,NSAMP
      DATA(I)=FLOAT(INDATA(I))/4.
   10 CONTINUE
      IF((KKK.EQ.3).AND.(NEWI.NE.LBLK))LREC=NEWI-2*NSAMP
C
CC    NORMALIZE (0 TO 1) TO DISPLAY
C
      DO 12 I=1,LREC
      DATA(I)=(DATA(I)-DMIN)/DMAX2
   12 CONTINUE
C
CC    FORM THE ARRAY INDATA WITH GRAPHICS WORDS
C
      L=1
  996 CONTINUE
      CALL DGINIT(IDEV,IGDIR,5,IER)
      IF(IER.NE.0) OUTPUT(101) IER,'D1'
      T(1)=TIME
      DO 19 I=1,NDIS
      TIME=TIME+(((DATA(L)*DMAX2)+DMIN)/1000000.)
```

```
      IF(I.EQ.(NDIS/2))T(2)=TIME
      IF(I.EQ.NDIS) T(3)=TIME
   19 CONTINUE
      ENCODE(96,320,ITEXT)T(1),T(2),T(3)
  320 FORMAT(28X,F6.3,12X,F6.3,12X,F6.3)
      CALL TEXTO(IDEV,ITEXT,24,22,1,1,3,IER)
      IF(IER.NE.0)OUTPUT(101)IER,'TTIME'
      INDATA(1)=IHEAD(0,10)
      INDATA(2)=IPACK(-.5,.5,0)
      INDATA(3)=IPACK((1./DIV)-.5,DATA(L),0)
      DO 6 I=2,NDIS
      INDATA(I+2)=IPACK((I/DIV)-.5,DATA(L+I-1),1)
    6 CONTINUE
      NWORD=NDIS+2
C
C   DRAW ON SCREEN
C
      CALL GRAPHC(IDEV,IAXIS,9,1,IER)
      IF(IER.NE.0)OUTPUT(101)IER,'G1'
      CALL GRAPHC(IDEV,INDATA,NWORD,2,IER)
      IF(IER.NE.0)OUTPUT(101)IER,'G2'
      N=N+NDIS
   80 CALL FNS(IDEV,ISW,IER)
      IF(IER.NE.0) OUTPUT(101) IER,'F1'
      IF(LLS(ISW,15).LT.0) GO TO  18
      IF(LLS(ISW,16).LT.0) GO TO 995
      GO TO 80
   18 L=L+NDIS
      IF(L.LE.(NSAMP-NDIS+1)) GO TO 996
      KKK=KKK+1
      IF(KKK.GT.3)NBLK=NBLK+1;GO TO 999
      GO TO 998
  995 STOP
      END
-LOAD XF,MAP
-DATA
```

BIBLIOGRAPHY

1. Bartels, Jr. and Chapman, S., Geomagnetism, 2d ed., vi, Oxford University Press, 1951.

2. Campbell, W. H. and Matsushita, S., Physics of Geomagnetic Phenomena, v. 1, 2, Academic Press, 1967.

3. Air Force Cambridge Research Laboratories, Handbook of Geophysics and Space Environments, p. 11-1 - 11-61, 1965.

4. Bloom, A. L., "Optical Pumping," Scientific American.

5. Hartmann, F., "Resonance Magnetometers," IEEE Transactions on Magnetics, v. MAG-8, p. 66-75, March 1972.

6. Grivet, P. A. and Malnar, L., "Measurement of Weak Magnetic Fields by Magnetic Resonance," Advances in Electronics and Electron Physics, v. 23, p. 39-151, 1967.

7. Bloom, A. L., "Principles of Operation of the Rubidium Vapor Magnetometer," Applied Optics, v. 1 no. 1, p. 61-68, January 1961.

8. Blevins, S. L., Cabiness, P. C., and Slocum, R. E., "Self Oscillating Magnetometer Utilizing Optically Pumped Helium," The Review of Scientific Instruments, v. 42, no. 6, June 1971.

9. Campbell, W. H. and Zimmerman, J. E., "Tests of Cryogenic SQUID for Geomagnetic Field Measurements," Geophysics, v. 40 no. 2, p. 269-284, April 1975.

10. Langan, L., Lynch, V. M., and Slack, H. A., "The Geomagnetic Gradiometer," Geophysics, v. 32 no. 5, p. 877-892, October 1967.

INITIAL DISTRIBUTION LIST

		No. Copies
1.	Defense Documentation Center Cameron Station Alexandria, Virginia 22314	2
2.	Library, Code 0212 Naval Postgraduate School Monterey, California 93940	2
3.	Department Chairman, Code 52 Department of Electrical Engineering Naval Postgraduate School Monterey, California 93940	2
4.	Assoc. Professor George L. Sackman Department of Electrical Engineering Naval Postgraduate School Monterey, California 93940	3
5.	LT C. L. Xefteris 4753 Red Coat Road Virginia Beach, Virginia 23455	1